

Revisiting large-scale interception patterns constrained by a synthesis of global experimental data

Feng Zhong^{1,2}, Shanhui Jiang^{2,3}, Albert I.J.M. van Dijk⁴, Liliang Ren^{2,3}, Jaap Schellekens⁵, and Diego G. Miralles¹

5 ¹Hydro-Climate Extremes Lab (H-CEL), Ghent University, Ghent, 9000, Belgium

²State Key Laboratory of Hydrology-Water Resources and Hydraulic Engineering, Hohai University, Nanjing 210098, China

³College of Hydrology and Water Resources, Hohai University, Nanjing, China

⁴Fenner School of Environment & Society, Australian National University, ACT, Australia

⁵Planet Labs, PBC, Haarlem, the Netherlands

10 *Correspondence to:* Diego G. Miralles (diego.miralles@ugent.be); Liliang Ren (rll@hhu.edu.cn)

Abstract. Rainfall interception loss remains one of the most uncertain fluxes in the global water balance, hindering water management in forested regions and precluding an accurate formulation in climate models. Here, a synthesis of interception loss data from past field experiments conducted worldwide is performed, resulting in a meta-analysis comprising 166 forest sites and 17 agricultural plots. This meta-analysis is used to constrain a global process-based model driven by satellite-observed vegetation dynamics, potential evaporation and precipitation. The model considers subgrid heterogeneity and vegetation dynamics, and formulates rainfall interception for tall and short vegetation separately. A global, 40-year (1980–2019), 0.1° spatial resolution, daily temporal resolution dataset is created, analysed and validated against in situ data. The validation shows a good consistency between the modelled interception and field observations over tall vegetation, both in terms of correlations and bias. While an underestimation is found in short vegetation, the degree to which it responds to in situ representativeness errors and difficulties inherent to the measurement of interception in short vegetated ecosystems is unclear. Global estimates are compared to existing datasets, showing overall comparable patterns. According to our findings, global interception averages to 73.81 mm yr^{-1} or $10.96 \times 10^3 \text{ km}^3 \text{ yr}^{-1}$, accounting for 10.53% of continental rainfall, and approximately 14.06% of terrestrial evaporation. The seasonal variability of interception follows the annual cycle of canopy cover, precipitation, and atmospheric demand for water. Tropical rainforests show low intra-annual vegetation variability, and seasonal patterns are dictated by rainfall. Interception shows a strong variance among vegetation types and biomes, supported by both the modelling and the meta-analysis of field data. The global synthesis of field observations and the new global interception dataset will serve as a benchmark for future investigations, and facilitate large-scale hydrological and climate research.

1. Introduction

30 Vegetation rainfall interception loss (I) is the volume of rainfall captured by plant surfaces and evaporated back into the atmosphere without reaching the ground. It plays a pivotal role in the hydrological cycle and land–atmosphere interactions, representing a net 'loss' of water for ecosystems, and a net 'gain' of moisture for the atmosphere. Its accurate monitoring is therefore not only crucial for water and forest management, but also for climatic and meteorological applications. In forests, the intercepted rainfall by plant canopies typically accounts for 10–30% of the gross rainfall (P), but it may reach up to 50%
35 in dense boreal forests (Molina and Del Campo, 2012; Zabret et al., 2017; Hassan et al., 2017) and montane rainforests (Tarazona et al., 1996; Schellekens et al., 2000). Despite this importance, I has been traditionally overlooked by global hydrological models, and in ecosystem-scale research dedicated to exploring evaporation and its partitioning based on eddy-covariance data (Stoy et al., 2019).

Nonetheless, decades of experimental research have contributed to increasing our process-understanding of this flux,
40 especially over forests (Van Dijk et al., 2015). Experiments conducted either at the single tree or plot level have allowed the design of multiple models, ranging from fully empirical I vs. P regressions (Zhang et al., 2017; Zheng et al., 2018), to stochastic models (Calder et al., 1986; Calder, 1996; Xiao et al., 2000), to process-based formulations (Rutter et al., 1971; Gash et al., 1980; Valente et al., 1997; Van Dijk and Bruijnzeel, 2001b). New approaches for estimating I have also been developed recently, including, for example, a physically-based model only forced by precipitation (Návar, 2019, 2020) or a
45 novel soil moisture-based method used to estimate storage capacity assuming that infiltration begins only after interception storage is full (Acharya et al., 2020). Besides, improved technology and process understanding have allowed increasingly detailed studies on I in the field, that range from investigating the intrastorm-scale interception (Reid and Lewis, 2009; Iida et al., 2017), to assessing the influence of canopy structure (Ginebra-Solanellas et al., 2020; Yan et al., 2021) and climate factors (Pérez-Suárez et al., 2014; Zabret et al., 2018). Such detailed research provides an opportunity for further insights
50 into the interception process, but the requirement for information about specific rainfall properties (e.g., raindrop size and velocity) and vegetation characteristics (e.g., stem density and litter layer thickness) challenges the consideration of these advances in global model applications.

Global I estimation is essential for understanding the land influence on climate and the large-scale availability of water resources. Current global land surface models as well as remote sensing-based approaches typically rely on Rutter-like
55 formulations (Rutter et al., 1971; Rutter et al., 1975), which track the flow and storage of precipitation through different compartments across vegetation. Of these formulations, the Gash analytical model (Gash et al., 1980; Gash et al., 1995), and subsequent adaptations (Valente et al., 1997; Van Dijk and Bruijnzeel, 2001b), have been particularly popular for large-scale applications, owing to their low input data requirements and daily scale simulation with the assumption of one storm per rain day. Based on the adaptation by Valente et al. (1997), Miralles et al. (2010) presented the first global interception model
60 solely based on satellite data as input, which was later applied, for instance, to benchmark reanalysis products (Reichle et al., 2011) and climate models (Yang et al., 2019). Likewise, the adapted version of the Gash analytical model proposed by Van

Dijk and Bruijnzeel (2001b) – hereafter referred to as vD–B model – has witnessed great success in recent years, largely due to its parsimonious parameterization of canopy cover and storage capacity, and its applicability to crops and other vegetation types beyond trees. This formulation has been successfully applied in remote sensing models (Zhang et al., 2016a; Zheng and Jia, 2020) and continental to global landscape hydrological models (Van Dijk, 2010; Wallace et al., 2013; Van Dijk et al., 2013). Most of these studies do not provide details about parameterization, and when values for these parameters are reported, they are generally taken from limited literature review exercises and often lack formal evaluations. These parameters, pertaining to either canopy structure or climatological conditions, are frequently considered as a constant due to the scarcity of measurements, whereas their spatial and temporal variability can still be very large (Deguchi et al., 2006; 65 Fathizadeh et al., 2018).

Despite these efforts, I remains one of the most uncertain fluxes in the global water balance (Dorigo et al., 2021). However, the valuable data and knowledge gained from field campaigns worldwide provides a unique opportunity to constrain and inform global I modelling. To date, this opportunity has not been exploited fully, partly due to the difficulties inherent to data collection and harmonisation of the hundreds of experimental campaigns conducted over the past decades. Unlike for 70 eddy-covariance, lysimeters or sap-flow measurements, no international observational network exists for I , and past campaigns are based on inconsistent measurement methods and limited observational periods. The development of a global-scale synthesis of parameters and field observations remains thus crucial for large-scale studies of interception loss. Despite the paucity of these experimental data, we already know from past campaigns that the heterogeneity in I induced by different vegetation types is large (Waterloo et al., 1999; Pérez-Suárez et al., 2014; Wang and Wang, 2020), which implies that 75 subgrid parameterization and validation are needed in global models. In general, forests can intercept more rainfall than short vegetation under the same weather conditions, due to their higher storage capacity and evaporation rates during rainfall. Therefore, the sensitivities shown by analytical models to the parameterizations of storage capacity and wet canopy evaporation rates should differ for different land cover types (Limousin et al., 2008; Linhoss and Siegert, 2016; Liu et al., 80 2018; Fathizadeh et al., 2018; Ma et al., 2019). Finally, a comprehensive synthesis of past field campaigns could also 85 provide an opportunity to validate global model performance in a much more extensive way than what has been done in the past.

Therefore, this study presents a synthesis of interception loss data from past field campaigns worldwide (Sect. 2.1 and Sect. 4), with the goal of using it to constrain a global vD–B model driven by satellite-observed vegetation dynamics, potential evaporation and precipitation data (Sect. 3). The model considers subgrid heterogeneity and vegetation dynamics, and 90 formulates rainfall interception for tall and short vegetation separately. A global, 40-year (1980–2019) I dataset is generated at a daily temporal and 0.1° spatial resolution, which is validated against past field observations (Sect. 5.1) and compared to existing global datasets (Sect. 5.5). The I patterns are analysed in terms of global magnitude and spatial variability (Sect. 5.2), seasonal dynamics (Sect. 5.3), and differences between biome types (Sect. 5.4).

2. Data

95 2.1 Field campaign data

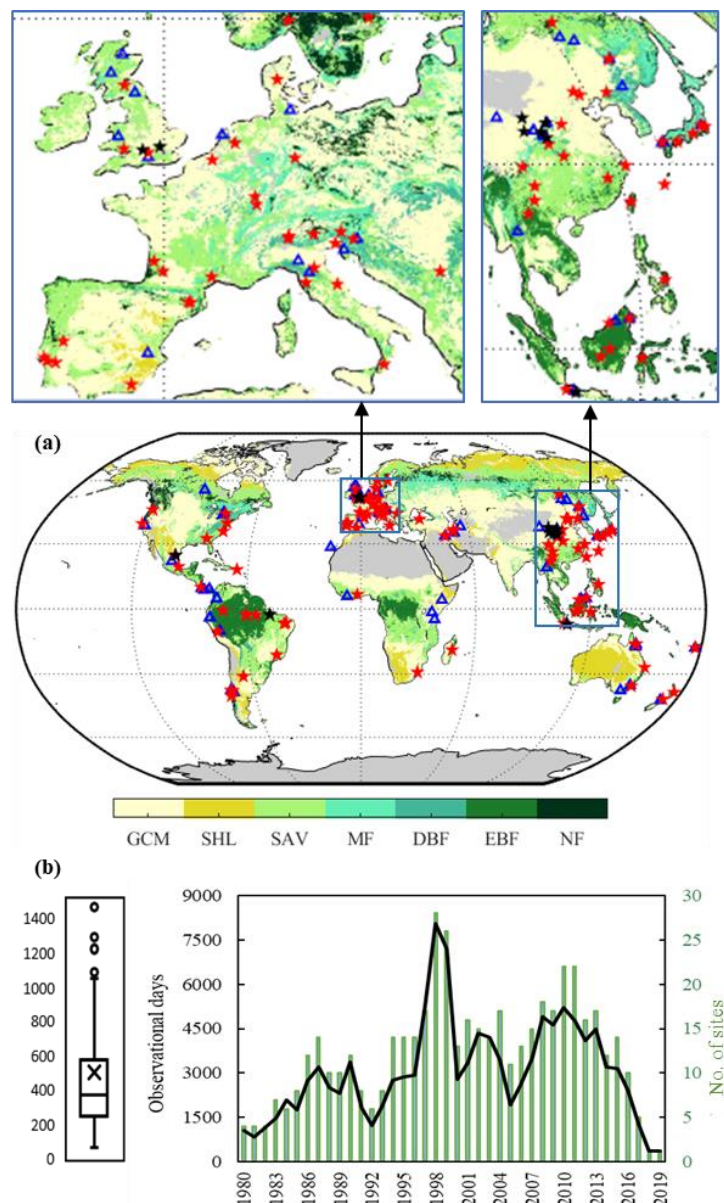
A comprehensive meta-analysis of previous interception loss field campaigns provides an extensive archive of data to parameterize and/or validate model estimates over multiple biome types. We search for peer-reviewed articles and academic dissertations reporting rainfall interception or rainfall partitioning published before September 2021 on Google Scholar, Web of Science, China National Knowledge Infrastructure, and in reference lists of identified primary studies or review papers. In 100 this study, we mainly focus on parameters related to vegetation storage capacity and wet canopy evaporation rate, and field observations of interception, precipitation and rainfall rates.

We synthesis the partitioning of incident rainfall into interception, stemflow and throughfall by trees and shrubs at the global scale. In total, 268 observational records are collected from 169 independent publications. Most of them span up to 2 years. To ensure the representativeness of the observations and minimise their inconsistencies with estimations, records are 105 discarded if (a) the campaign lasts less than half a year; (b) they include cloud and/or snow interception; (c) they are affected by abundant epiphytes; (d) they belong to city parks; (e) they are based on insufficient measurements (less than 10 throughfall gauges and no assessment of stemflow) or fixed rain gauges. After such screening, 193 observations from 125 sites are retained for validation. The locations of experimental sites are shown in Fig. 1. All the metadata collected from literature is given in Supplement.

110 2.2 Gridded data

Several observational datasets are used to compute I at the global scale based on a global vD–B model (Sect. 3) parameterised and constrained using the in situ data (Sect. 4). To characterise canopy cover fraction (c), global Vegetation Continuous Fields (VCF) products from the Moderate Resolution Imaging Spectroradiometer (MODIS) MOD44B and the Making Earth System data records for Use in Research EnvironmentS (MEaSURES) are selected. Both products are 115 generated on an annual basis and provide the percentage of each gridcell covered by each of the following land cover classes: tall vegetation (i.e. tree canopies), short vegetation (i.e. non-tree vegetation), and bare ground. The MEaSURES product (Hansen and Song, 2017) is created with a bagged linear model algorithm based on surface reflectance and brightness temperature from the Advanced Very High Resolution Radiometer (AVHRR) and MODIS, covering a 35-year record from 1982 to 2016. The MOD44B product (Dimiceli et al., 2017) is retrieved from MODIS on the basis of regression tree models 120 created using machine learning, and spans from 2000 to near present. In order to have a long and consistent data series, a cumulative density function matching approach of Reichle and Koster (2004) is applied. This removes systematic differences between the two, and yields a merged VCF dataset covering 1982–2019. For the period 1980–1981, the VCF of 1982 is used. Moreover, the MODIS Land Cover Product (MCD12C1) (Sulla-Menashe et al., 2019), based on the International 125 Geosphere–Biosphere Programme (IGBP) classification, is selected to extract the spatial distribution and fractions of forest (FF , including Evergreen Needleleaf Forests, Evergreen Broadleaf Forests, Deciduous Needleleaf Forests, Deciduous

Broadleaf Forests, Mixed Forests, Woody Savannas and Savannas) and non-forest (Closed Shrublands, Open Shrublands, Grasslands, Croplands, Cropland/Natural Vegetation Mosaics, and Permanent Wetlands) ecosystems per pixel for validation purposes (see Sect. 5.1).



130 **Figure 1. (a) Spatial distribution of experimental sites and vegetation cover types.** Red and black stars represent tall vegetation
 and short vegetation sites retained for validation (respectively), while blue triangles are discarded sites. Vegetation cover is based
 on the IGBP classification of MCD12C1 corresponding to 2001, including Evergreen Needleleaf Forests and Deciduous Needleleaf
 Forests (NF), Evergreen Broadleaf Forests (EBF), Deciduous Broadleaf Forests (DBF), Mixed Forests (MF), Woody Savannas and
 Savannas (SAV), Closed Shrublands and Open Shrublands (SHL), Grasslands, Croplands and Cropland/Natural Vegetation
 Mosaics (GCM). (b) Observational days of field experiments (left), and the number of days and sites each year (right).

135

Fraction of absorbed Photosynthetically Active Radiation (*fPAR*) and Leaf Area Index (*LAI*) retrievals are taken from the MODIS V6 MCD15A3H product. This newest version at 500 m resolution benefits from an improved biome map from the high spatial resolution MODIS Land Cover Product (MCD12Q1), which provides an accurate parameter estimation related to vegetation structural types for three-dimensional radiative transfer formulations (Yan et al., 2016a). To discriminate
140 between tall vegetation and short vegetation fractional covers, and obtain representative *fPAR* and *LAI* for each of these two fractions at 0.1° resolution, 250 m resolution MOD44B data is used to select the values of *fPAR* and *LAI* from the 'purest' high-resolution pixels; for instance, the *fPAR* for tall vegetation in a certain 0.1° gridcell is the average of the 500 m resolution *fPAR* values for the pixels with a fraction of tall vegetation >98th percentile in the 0.1° gridcell. This work is done in Google Earth Engine, and its quality flag is used to exclude low-accuracy observations contaminated by clouds and snow.
145 The original 4-day resolution is temporally smoothed and gap filled based on the Temporal Smoothing and Gap Filling (TSGF) method proposed by Verger et al. (2011). A 7-year climatology is applied to fill gaps with missing data longer than 64 days. The gap-free daily time series are achieved with linear interpolation. The daily climatology of *fPAR* and *LAI* based on 2003–2007 is used for the period prior to MODIS.

Taking advantage of the complementary strengths of gauge-, satellite-, and reanalysis-based data, the Multi-Source
150 Weighted-Ensemble Precipitation (MSWEP v2.8) data (Beck et al., 2019) is selected as the precipitation forcing in this study. The climatological rainfall rate (*R*) during *P* events is also derived from the 3-hr MSWEP, by taking the maximum accumulated volume over the 3-hr periods at the monthly time scale. To mask out snow periods, observations of Snow-Water Equivalent (*SWE*) from the European Space Agency (ESA) GLOBSNOW product (Luoju et al., 2013) are used over the Northern Hemisphere; the monthly *SWE* climatology product from the National Snow and Ice Data Centre (NSIDC)
155 (Armstrong et al., 2005) is used for the Southern Hemisphere. The Priestley and Taylor-based potential evaporation (*E_p*) from the Global Land Evaporation Amsterdam Model (GLEAM, Miralles et al., 2011b) version v3.5a (Martens et al., 2017) is selected as a proxy of mean wet canopy evaporation (*E_C*) for short vegetation. Natural neighbour interpolation is applied in resampling the datasets from their original spatial resolution to a common 0.1° global grid. An overview of all gridded datasets used can be found in Table 1.

160 **Table 1. Overview of the selected forcing datasets used in the global application of the vD–B model.**

Variables	Dataset	Resolution	Period	References
<i>P</i>	MSWEP v2.8	Daily; 0.1°	1979–2020	Beck et al. (2019)
<i>R</i>	MSWEP v2.8	3-hour; 0.1°	1979–2020	Beck et al. (2019)
<i>VCF</i>	MOD44B v6.1	Yearly; 250m	2000–2019	Dimiceli et al. (2017)
	MEaSURES	Yearly; 0.05°	1982–2016	Hansen and Song (2017)
<i>FF</i>	MCD12C1	Yearly; 0.05°	2001–2019	Sulla-Menashe et al. (2019)
<i>fPAR & LAI</i>	MCD15A3H v6	4-day; 500m	2002–2020	Yan et al. (2016a); (2016b)
<i>E_p</i>	GLEAM v3.5a	Daily; 0.25°	1980–2020	Miralles et al. (2011b); Martens et al. (2017)
<i>SWE</i>	GLOBSNOW L3av2 +NSIDC v0.1	Daily; 0.25°	1980–2015	Luoju et al. (2013) Armstrong et al. (2005)

3. Model formulation

Most studies of I are focused on forest plots or single trees, often following the assumption that I in short vegetation ecosystems is less important, due to the lower aerodynamic conductance and weaker coupling to the atmosphere (David et al., 2006; Paço et al., 2009). However, short vegetation I cannot be ignored; the fraction of terrestrial evaporation that relates to 165 plant water consumption (transpiration) needs to be isolated from the entire evaporative flux to understand water use efficiency and the links to the carbon cycle (Miralles et al., 2020). Previous uses of the modified Gash model described by Van Dijk and Bruijnzeel (2001b) (i.e. the vD–B model) confirm its applicability to agricultural cropping systems (Van Dijk and Bruijnzeel, 2001a; Fernandes et al., 2017) and grasslands (Finch and Riche, 2010). In fact, the vD–B model has already 170 been applied to estimate I in tall and short vegetation ecosystems, both regionally (Cui and Jia, 2014; Cui et al., 2017) as well as globally (Zhang et al., 2016a; Zheng and Jia, 2020). The vD–B model is also implemented in the Australian Water Resources Assessment (AWRA) system (Van Dijk, 2010; Wallace et al., 2013) and the global WR3A/W3 models (e.g., Van Dijk et al. (2013); (2018); Schellekens et al. (2017)).

The vD–B model proposes several improvements to the assumptions and parameterization in the sparse Gash model (Gash et al., 1995; Valente et al., 1997). The main feature of the vD–B model is the incorporation of LAI to evaluate the influence of 175 vegetation structure and density on I . Analogous to the transmittance of light through the canopy considering the vegetation elements as opaque, c is approximated as an exponential function of LAI using Beer–Lambert's Law:

$$c = 1 - e^{(-\kappa \cdot C \cdot LAI / \mu)} \quad (1)$$

with κ being the extinction coefficient, and with the clumping index (C) and the cosine of the Sun zenith angle (μ) being set to unity in the vD–B model. Moreover, the canopy storage capacity (S) is assumed to be linearly related to LAI , instead of 180 being linearly related to c as in the sparse Gash model by Valente et al. (1997). These adaptations make I directly sensitive to temporal changes in LAI , thus providing insight into seasonal phenology influences. Furthermore, the vD–B model makes a modification to the questionable assumption that no water evaporates from stems before the canopy is saturated, through 185 treating the rainfall retained on stems similarly to that retained by the canopy. Under such assumptions, the storage capacity of canopies (S) and stems (S_S) can be integrated into a total storage capacity (S_V). Hence, the rainfall intercepted by canopies and stems is no longer strictly distinguished in the model calculations. The corresponding equations and parameters of the vD–B model are given in Table 2. For a detailed description of the conceptual framework and improvements please see Gash et al. (1995) and van Dijk and Bruijnzeel (2001b).

Recently, C is shown to be an important biophysical parameter in characterising the effective LAI as a function of the distribution and density of foliage within crowns using radiative transfer models (Béland and Baldocchi, 2021). The impacts 190 of clumping on transpiration and photosynthesis have also been evaluated in detail (Braghieri et al., 2019; 2020; 2021). Here, we exploit the value of $fPAR$ data in order to evaluate the impact of canopy structure and density on I without the need to

retrieve suitable values for C , μ and κ over different regions. Meanwhile, the approach allows the consideration of intra-annual dynamics in c :

$$c = VCF \cdot \left[\frac{fPAR_{daily}}{fPAR_{mean}} + K(s) \right] \quad (2)$$

195 where VCF is the (annual mean) fraction of vegetation cover, $fPAR_{daily}$ and $fPAR_{mean}$ are the daily and annual mean $fPAR$ for the corresponding land cover fraction (tall or short vegetation) within each pixel – see Sect. 2.2 for the data sources and pre-processing. $K(s)$ is a coefficient indicating the proportion of non-green vegetation, i.e., trunks, branches and necrotic leaves, a parameter similar to the stemflow partitioning coefficient (P_t) in Rutter and Gash models; values 0.028 (Gash et al., 1995; Zeng et al., 2000) and 0.010 (Návar et al., 1999) are chosen for tall and short vegetation, respectively. After applying
200 Eq. (2), spurious c values larger than unity are set to unity. Implicit to the approach of using $fPAR$ to compute the rainfall intercepting surface fraction (i.e. c) is the assumption that the light and rain penetration through the canopy is alike. Previous studies have shown that $fPAR$ and c can be derived using the same equation either from LAI (Majasalmi et al., 2017) or the Normalized Difference Vegetation Index ($NDVI$, Carlson and Ripley, 1997), and $fPAR$ exhibits strong linear correlation to c (Mu et al., 2018). For instance, in the Priestley and Taylor Jet Propulsion Laboratory (PT-JPL) model (Fisher et al., 2008), c
205 is assumed equal to light intercepted (not absorbed) by the vegetation fraction ($fIPAR$), and in the Penman–Monteith MODerate Resolution Imaging Spectroradiometer (PM-MOD) model (Mu et al., 2011), the $fPAR$ from MOD15A2 is directly used as a surrogate of c in estimating global terrestrial evaporation. Conversely, in the Penman–Monteith–Leuning (PML) model (Zhang et al., 2016a) and the ETMonitor model (Hu and Jia, 2015), both based on the model by Van Dijk and Bruijnzeel (2001b), c is calculated as a function of LAI following the Beer's law.

210 **Table 2. Equations and parameters in the original vD–B model and this study. In the original vD–B model, α is the energy exchange coefficient between canopy and atmosphere, and \bar{E}_a is a constant evaporation rate when α approaches infinity. The values of S_L and S_S in the original vD–B model come from van Dijk and Bruijnzeel (2001a), and the parameterisation in this study is based on the meta-analysis of past field campaigns. EBF, DBF, NF and others represent Evergreen Broadleaf Forests, Deciduous Broadleaf Forests, Needleleaf Forests, and other tall vegetation, separately.**

	The original vD–B model	This study	
		tall vegetation	short vegetation
<i>I</i> calculation			
For storms insufficient to saturate vegetation, i.e. $P \leq P'$	$I = c \cdot P$		$I = c \cdot P$
For storms sufficient to saturate vegetation, i.e. $P > P'$	$I = c[P' + (E_C/R)(P - P')]$		$I = c[P' + (E_C/R)(P - P')]$
Parameters			
Rainfall necessary to saturate vegetation, P' (mm)	$-[RS_V/(c \cdot E_C)]\ln(1 - E_C/R)$		$-[RS_V/E_C]\ln(1 - E_C/R)$
Vegetation cover fraction, c (-)	$1 - e^{(-\kappa \cdot LAI)}$		$VCF[fPAR_{daily}/fPAR_{mean} + K(s)]$
Vegetation storage capacity, S_V (mm)	$LAI \cdot S_L + S_S$		$LAI \cdot S_L + S_S$
Mean wet canopy evaporation rate, E_C (mm h ⁻¹)	$\{[1 - e^{(-\alpha \cdot LAI)}]\bar{E}_a\}/c$	0.32	E_p
Leaf storage capacity, S_L (mm)	0.077 for maize 0.042 for rice 0.049 for cassava	0.20 for EBF 0.18 for DBF 0.29 for NF 0.23 for others	0.10
Trunk/Stem capacity, S_S (mm)	0.001–0.012	0.09	0.03

215 Note: LAI and S_S are expressed per unit area of total land in the original vD–B model, while per unit area of canopy in this study.

In addition to c , other parameters in the global vD–B model include E_C , leaf storage capacity (S_L) and S_S . In this study, we take advantage of the large archive of field data collected from literature (Sect. 2.1) to select the most adequate values of E_C , S_L and S_S for different biomes (Sect. 4). The formulations and parameter values of the global vD–B model are provided in Table 2.

220 4. Meta-analysis and model parameterisation

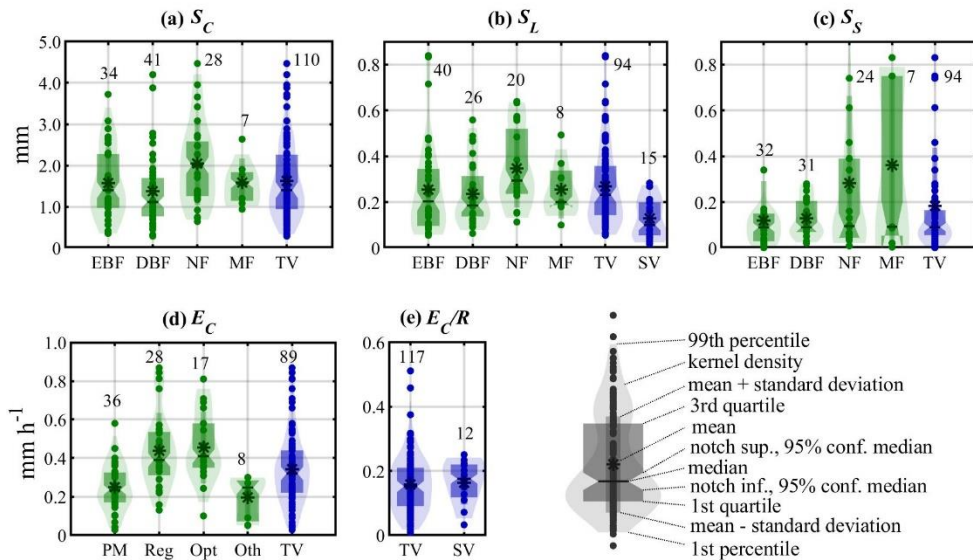
4.1 Vegetation storage capacity

Generally in the literature, canopy storage capacity is expressed either per unit of total area (S), canopy area (S_C) and leaf surface area (S_L). In most rainfall interception studies, S is assumed to be linearly related to S_C and c . S_C is often assumed to vary per vegetation type and is dependent on climate conditions. In nature, S_C is dependent on vegetation morphological characteristics such as leaf surface area, inclination and hydrophobicity (Garcia-Estringana et al., 2010; Holder, 2013; Ginebra-Solanellas et al., 2020), as well as meteorological variables like rainfall intensity, droplet size and wind (Hörmann et al., 1996; Klaassen et al., 1996; Sun et al., 2018, Gerrits et al., 2010). It may explain why the S_C values collected in previous campaigns can vary widely, from 0.35 mm (Valente et al., 1997) to 4.47 mm (Shi et al., 2010) – see Fig. 2a. The concepts of static/dynamic storage (Keim et al., 2006) and minimum/maximum storage (Xiao and Mcpherson, 2016) have been proposed to account for the storage changes driven by meteorological variables during specific rainfall events. Some studies suggest that LAI can be a valuable variable to explain the variability in S , and further study their potential relation using linear (Van Dijk and Bruijnzeel, 2001b; Deguchi et al., 2006; Wallace and McJannet, 2008), nonlinear (De Jong and Jetten, 2007; Mianabadi et al., 2019) and exponential (Wallace et al., 2013) regressions. Here, we revisit the relationship between S , LAI and c over multiple ecosystems based on previous studies (Fig. S1). A linear relationship between S and LAI is only found for short vegetation ($r=0.73$) and coniferous forests ($r=0.60$), while S shows a weak linear correlation to c only in broadleaf forest ($r=0.54\sim0.59$). Nonlinear regressions do not show a higher accuracy than linear regressions in the prediction of S (based on either LAI or c) over any ecosystems.

As the majority of studies focus on either S or S_C , c and LAI are collected to derive S_L indirectly under the assumption that canopy capacity is linearly related to LAI . As such, caution should be taken in calculating S_L that canopy capacity and LAI should be expressed in uniform scales, as LAI can be given in per unit of total land area or just canopy area which often have to be deduced from the context of the study. Based on traditional statistical analysis, needleleaf forest shows larger S_L with a median value 0.29 mm (95% confidence level 0.25–0.34 mm), while within other forest types S_L is similar; 0.20 (0.16–0.24), 0.18 (0.16–0.21) and 0.20 (0.18–0.22) mm are found for evergreen broadleaf forests, deciduous broadleaf forests, and mixed forests, respectively (Fig. 2b). The median value of 0.23 (0.20–0.27) mm for all forest types is much larger than the 0.10 (0.08–0.12) mm found for short vegetation plant functional types (i.e., crops, grass and shrubs). Stem storage capacity (S_S) is influenced by stem density, bark surface roughness, the arrangement of twigs and leaves, and epiphytes. Large discrepancies

are shown in reported studies with a range from 0.01 mm (Návar, 2013) to 0.83 mm (Chen et al., 2013). Often, S_s is obtained from an indirect, regression-based method in I simulations based on field observations (Gash and Morton, 1978; Gash, 1979; Lloyd et al., 1988). Compared to other variables like S_c , which can have a large influence, the sensitivity of I to S_s is fairly low (Liu et al., 2018; Ma et al., 2019), being even ignored in some early studies (Lundgren and Lundgren, 1979; Lankreijer et al., 1993). Despite the strong range of variability in the values of S_s reported in past field campaigns, the median value around 0.09 mm is found for all tall vegetation types (Fig. 2c). Reviewing the limited literature on short vegetation S_s , the values from mixed crops, i.e. maize, rice and cassava (Van Dijk and Bruijnzeel, 2001a), hedgerow (Herbst et al., 2006), and thornscrub (Návar and Bryan, 1994; Návar et al., 1999) are remarkably similar, ranging from 0.01–0.05 mm (Table S1).
 250 Based on the results of this comprehensive meta-analysis, the median value is used in the execution of the global vD–B model over different vegetation types (Sect. 3), as shown in Table 2.

255



260 **Figure 2. Violin plots of parameter statistics based on a meta-analysis of 183 field campaigns. (a, b, c) Parameters related to**
265 storage capacity, i.e., canopy storage capacity per unit of canopy area (S_c), leaf area (S_L), and stem storage capacity (S_s). (d, e) Parameters related to evaporation, i.e., wet canopy evaporation rate (E_c) and the ratio between wet canopy evaporation rate and rainfall rate (E_c/R). Green bars are used for plant functional types, including Evergreen Broadleaf Forests (EBF), Deciduous Broadleaf Forests (DBF), Evergreen Needleleaf Forests and Deciduous Needleleaf Forests (NF) and Mixed Forests (MF). Blue bars represent the statistics for all tall vegetation (TV) and short vegetation (SV) plant functional types. The methods to obtain E_c in (d) include the Penman–Monteith equation (PM), Regression (Reg), Optimization (Opt) and Other (Oth) methods. Labels with numbers represent the number of field observations.

4.2 Wet canopy evaporation rate

E_c is usually estimated from the canopy energy balance or the surface water budget. A conventional method is to derive E/R from the slope of the linear regression of observed evaporation (i.e. I) against observed P (Gash, 1979; Klaassen et al., 1998; Wallace and McJannet, 2006). Alternatively, based on meteorological data (e.g., net radiation, temperature, humidity and

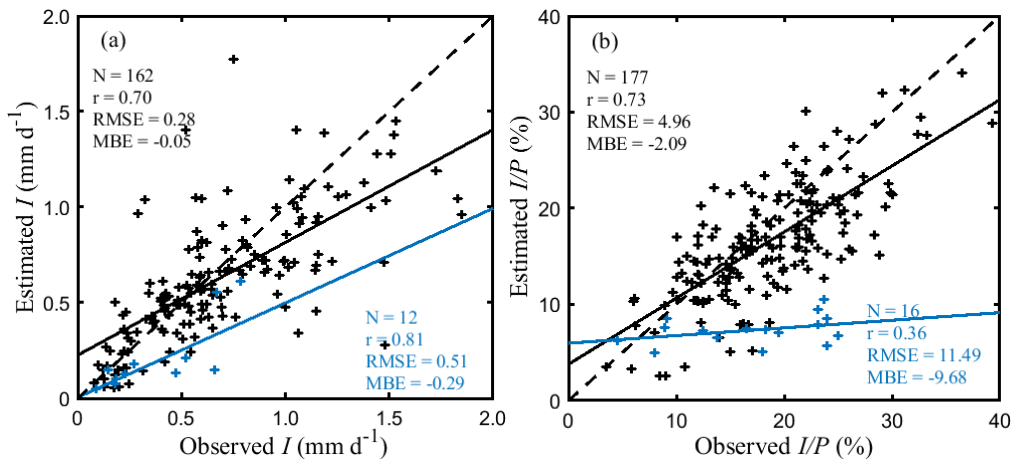
270 wind speed), the Penman–Monteith equation (PM) (Monteith, 1965) is often applied to estimate E_C from wet canopies, with the surface resistance being set to zero, essentially equating to the original Penman equation (Penman, 1948). The main drawback in applying PM is systematic underestimation of E_C due to the underestimation of the aerodynamic conductance, and to a lesser extent, the available energy for wet canopy evaporation (Holwerda et al., 2012; Van Dijk et al., 2015). Considering that E_C is driven largely by water vapour pressure deficit and aerodynamic conductance, to a smaller extent by 275 available energy, Pereira et al. (2009; 2016) suggested that Dalton-type equation, a simple water vapour diffusion equation determined by air wet bulb temperature, could be used to estimate E_C from wet sparse canopies. Besides, E_C can be optimised by minimising the squared differences between the paired simulated and observed I (Ghimire et al., 2012; Wallace et al., 2013; Fan et al., 2014). Finally, less commonly, E_C can be estimated on the basis of eddy-covariance or Bowen-ratio 280 measurements (Hörmann et al., 1996; Holwerda et al., 2012; Ringgaard et al., 2014). All these methods suffer from their own potential issues and uncertainties (Van Dijk et al., 2015).

Before comparing the E_C from previous studies published in the literature, it is essential to clear their units and scale them correctly. The evaporation obtained from the PM and Dalton-type equation represents the rate per unit area of canopy cover (i.e., E_C), but the value derived from regression is expressed per unit of total area (E). When it comes to estimating E_C on the basis of eddy-covariance or Bowen-ratio measurements, it is important to note the influence of all components of 285 evaporation from canopies and bare soils. Although transpiration tends to be very low during rain (Gash and Stewart, 1977), Ringgaard et al. (2014) suggested restricting this method to canopies with sufficient cover when evaporation from soils approaches zero. Here, the value of E_C is obtained by dividing E by cc for the studies in which only E is given. The synthesis of all these studies shows that the values of E_C predicted from regression and optimization methods have greater fluctuations (Fig. 2d), and they can be several times larger than those based on PM and other energy balance based methods (i.e. Dalton 290 equation, eddy covariance and Bowen ratio). This discrepancy is recognised and critically discussed by Van Dijk et al. (2015). For tall vegetation, the median value of E_C is 0.32 mm hr^{-1} with 95% confidence level $0.29\text{--}0.36 \text{ mm hr}^{-1}$. For short vegetation, E_C exhibits large variability, from 0.09 mm hr^{-1} for *Potentilla fruticosa* in China (Zhang et al., 2018) to 2.96 mm hr^{-1} for *thornscrub* in Mexico (Návar et al., 1999), and is on average slightly higher than that for tall vegetation. Besides, in terms of the ratio of E_C to R , low vegetation has a higher median value and a smaller range of variability (see Fig. 2e). We 295 note, however, that the short vegetation data comes only from 8 publications (Table S4). These findings seem to contradict the expectations of lower evaporation rates over short vegetation types (see e.g., Van Dijk et al. 2015), likely due to limitations in the number of short vegetation campaigns and the lack of representation of grasslands (in particular) where interception measurements are impractical. In those ecosystems, E_C is expected to be lower due to the higher aerodynamic resistance, presenting analogous rates to those of transpiration in similar weather conditions (David et al., 2006). Based on 300 this assumption, potential evaporation (E_p) is selected as a proxy of E_C for short vegetation in the execution of the global vD–B model (Sect. 3), despite the high E_C from the 8 short vegetation campaigns. For tall vegetation, the median value from this comprehensive meta-analysis of 50 studies is used, as shown in Table 2.

5. Results and discussion

5.1 Validation

305 The validation of the global vD–B model estimates of I is performed by comparison to the 193 field I observations. We note that while the parameterization in Sect. 4 also uses the field campaign data, the calibration is not performed per site but globally, so the comparison against the field observations to evaluate model performance appears adequate. A major challenge is the need to account for differences in forest cover between the 0.1° resolution grid cells and the study sites, bearing in mind that field observations are usually taken in local forest or shrubland plots whose density may not be 310 representative of that of the 0.1° resolution grid cell. For most natural forest stands, gaps exist between and within tree crowns, so standardising the pixel I estimates by c might result in an overestimation with respect to the field data. Conversely, dividing the pixel estimates by FF (instead of c) might result in an underestimation, especially when the 315 interception experiment is carried out only under specific trees. In order to allow for a fair comparison, we explore the characteristics of the individual field campaigns (e.g., vegetation types, observed c and LAI , throughfall measurement method, etc.). Standardisation by c is used for campaigns based on individual tree observations, when throughfall gauges are positioned beneath tree canopies only, or where c exceeds FF within the pixel; for all other sites, standardisation by FF is used. The correspondence between the observed and modelled I for all sites is shown in Fig. 3.



320 **Figure 3. Field validation. (a) I in mm d^{-1} , (b) I/P in %.** Black and blue scatters represent the stand-scale simulations of tall vegetation and short vegetation, respectively.

In tall vegetation ecosystems, both I (mm d^{-1}) and I/P (%) generally agree well with field observations, with correlation coefficients (r) of 0.70 and 0.73, respectively. A slight underestimation is shown by the mean bias error (MBE) of -0.05 mm d^{-1} for I and -2.09 % for I/P . This underestimation mainly occurs for high I values associated with high-advection coastal forests (Schellekens et al., 1999; Sadeghi et al., 2015; Fathizadeh et al., 2018) (Fig. S2). Similar validation results are found 325 over different forest types (Fig. S3), except for mixed forests where the performance is lower. The accuracy of estimates is strongly influenced by P (Sadeghi et al., 2015; Fathizadeh et al., 2018), which may explain some discrepancies in I and be

attenuated when expressing the results as I/P (Fig. S4). The slight underestimation may also relate to the assumption of one storm per rainy day in the daily application of Gash-type models. A precipitation event-scale validation can also be performed using the few field campaigns in which P and I have reported for individual events. Figure S5 shows the comparison between daily estimates from the global vD–B model and event-based observations reported by Link et al. (2004) in a temperate needleleaf forest in southwestern Washington, USA and by Chen and Li (2016) in a subtropical evergreen broadleaf forest in Taiwan, China. Here, events spanning more than 24 hr are not included. These two sites are well represented due to a good consistency of pixel-based vegetation cover compared to their site-level descriptions, even though I during the largest P events is underestimated by the model, probably affected by the daily scale of our simulations. A good agreement is found between the daily estimated I/P and event-based observed I/P , and significant negative logarithmic relationships are shown between I/P and P as described by Sadeghi et al. (2015).

For short vegetation interception, the estimated I has a good consistency with observations ($r=0.81$) but shows a larger underestimation ($MBE=-0.29 \text{ mm d}^{-1}$). Moreover, a low correlation is found between estimated and observed I/P ($r=0.36$). This lower performance is likely related to the errors derived from the modelling, measurement and validation, in addition to the limited number of short vegetation studies. From the modelling perspective, the underestimation of E_C related to the lower values of E_p (Sect. 4.2) explains the lower estimates of short vegetation interception. Besides, although the study species (e.g., shrubs, sugarcane, maize, etc.) from limited publications are defined here as 'short vegetation', they are all tall enough to fit funnels or gutters under them. Hence, these studies normally report higher I and I/P , and may not be representative for global short vegetation ecosystems, especially grasslands, that have a weaker coupling to the atmosphere and may experience shelter effects from the overstorey tall vegetation (Carlyle-Moses et al., 2010). For example, the measured I/P around 24% in hedgerows (Herbst et al., 2006) and sugarcane fields (Fernandes et al., 2017), is of similar magnitude with that typically reported in forests, and much higher than our estimates of 10.48%, 8.56% in these sites (Fig. 3). Waterloo et al. (1999) found grass interception was only about 4.53% of P in Fiji, which is, in fact, slightly lower than our estimates of 6.19%. Note as well that most observations in past campaigns come from single species of shrubs (Zhang et al., 2018) and crops (Finch and Riche, 2010; Zheng et al., 2018; Nazari et al., 2020), and that past studies have found large variability in I for different short vegetation species, even when exposed to the same climate. For instance, Zhang et al. (2016b) reported I/P values of 29.1% and 17.1% for *Caragana korshinskii* and *Artemisia ordosica* in the Shapotou Desert (China). Likewise, Zhang et al. (2017) reported 24.9% and 19.2% for two xerophytic shrub communities (dominated by *Hippophae rhamnoides* and *Spiraea pubescens*) in the Loess Plateau. Hence, rainfall interception may have high subgrid heterogeneity due to the large spatial complexity of biome compositions. The observed I from certain species may, therefore, not be representative for the whole grid. Finally, the average I/P values over low vegetated regions compare well with the findings by Wang-Erlandsson et al. (2014) based on a hydrological land-surface model.

5.2 Magnitude and spatial variability

The global distribution of I is shown in Fig. 4, and its seasonal-mean latitudinal variations are presented in Fig. 5. During the 360 40-year period 1980–2019, the estimated global average I is 73.81 mm yr^{-1} or $10.96 \times 10^3 \text{ km}^3 \text{ yr}^{-1}$, accounting for 10.53% of continental P and representing 14.06% of continental evaporation (taking GLEAM v3.5a evaporation as reference). As expected, most (68.70%) of I comes from tall vegetation, with a global average of 50.69 mm yr^{-1} or $7.52 \times 10^3 \text{ km}^3 \text{ yr}^{-1}$; this amounts to 6.12% of the continental precipitation, in agreement with the values reported by Miralles et al. (2011a). Although 365 short vegetation I is estimated to be substantially lower (bearing in mind the underestimation reported in Sect. 5.1 against past field campaigns), it still accounts for 4.20% of the continental P , and has a widespread influence across most of the land surface, deserving full consideration as a separate flux.

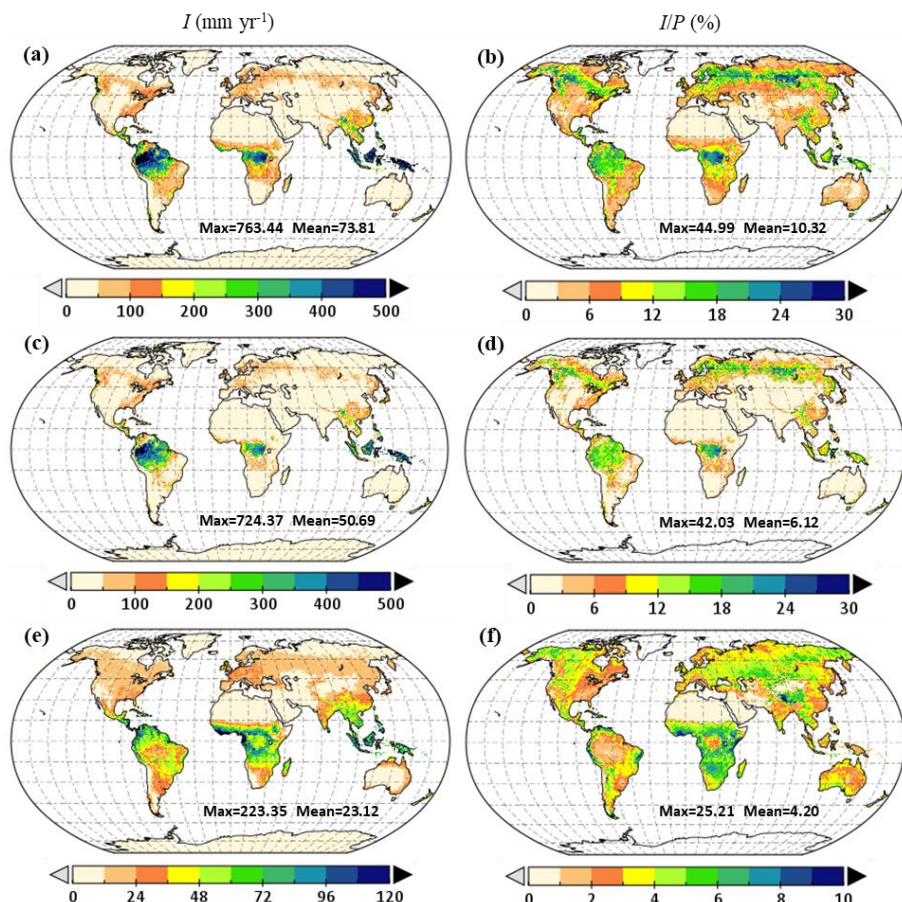


Figure 4. Global distribution of annual rainfall interception loss. Average I in mm yr^{-1} (a), and the contributions from tall (c) and short (e) vegetation. Average I/P (%) (b), and the contributions from tall (d) and short (f) vegetation.

370 In general, the spatial patterns of I agree well with the distribution of vegetation and precipitation. The high I volumes shown in tropical rainforests occur due to the combination of high P , dense evergreen vegetation, and high evaporation rates. High

values of I expressed in percentage of P , are estimated in both tropical and boreal regions, where c can approach 100%. Moreover, the lower rainfall rates in high latitude regions (Fig. S6) contribute to increasing I as a percentage of P by delaying canopy saturation. Tall vegetation dominates I in tropical and boreal latitudes, while the magnitude of short vegetation I can be comparable or even exceed that of tall vegetation in midlatitudes (15° N–40° N and 20° S–35° S) (Fig. 5a, b). This relates to low forest cover coverage of croplands, grasslands and shrublands over the south of Europe and North America, southeastern Asia, southern Africa and Australia. The highest annual I/P of short vegetation is shown in African drylands and the Tibetan Plateau (Fig. 4f). Note that the fluctuations around 40° S–60° S (Fig. 5) relate to the low fraction of land in those latitudes.

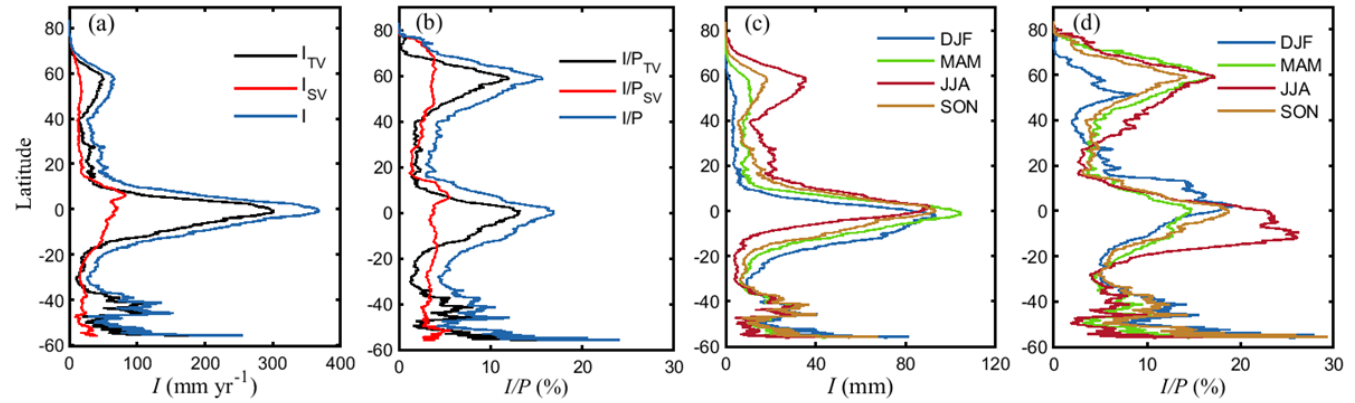


Figure 5. Variation of average I along different latitudinal bands. (a) I (mm yr^{-1}) for tall vegetation, short vegetation and their sum. (b) Same but for I/P (%). Seasonal patterns of I in mm yr^{-1} (c), and of I/P in % (d). DJF, MAM, JJA and SON represent December–February, March–May, June–August and September–November, respectively.

5.3 Seasonal patterns

The mean seasonal patterns of I are represented in a latitudinal profile (Fig. 5) and globally (Fig. 6). Overall, the seasonal variability of I follows the annual cycle of canopy cover, and rainfall volumes and intensity. The global averaged I and I/P are higher during boreal summer (June–August) and lower during austral summer (December–February) (Fig. 6). The largest seasonal variations in I are found in mid-high latitude regions (15° N–60° N and 10° S–30° S), with the highest values in summer and lowest in winter (Fig. 5c), following the seasonal green wave (Fig. S7). In tropical areas, the seasonal I is the highest in March–May, but it is rather stable throughout the seasons (Fig. 5c). However, when expressed in I/P , the latitudinal average shows higher values in June–August in mid-high northern latitude due to the increased c , and in the tropics south of the equator, i.e., Amazon and Congo forests, as a consequence of the reduced P in this time of the year (Fig. 5d, Fig. 6f). Similarly, higher I/P occurs in December–February over midlatitude regions in the Southern Hemisphere and in the tropics north of the equator. In mid-high latitude regions, characterised with high seasonal variations in vegetation cover (Fig. S7), the lower c results in both lower I and lower I/P during the dormant season (Fig. 5d).

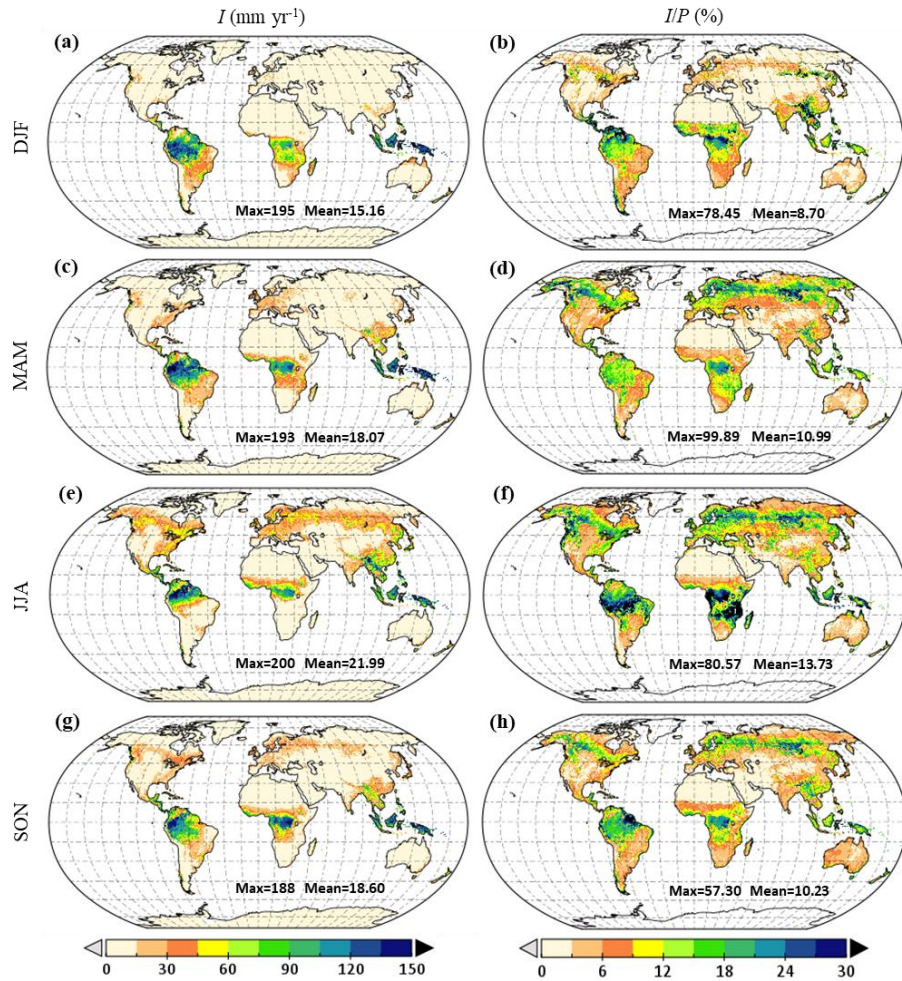
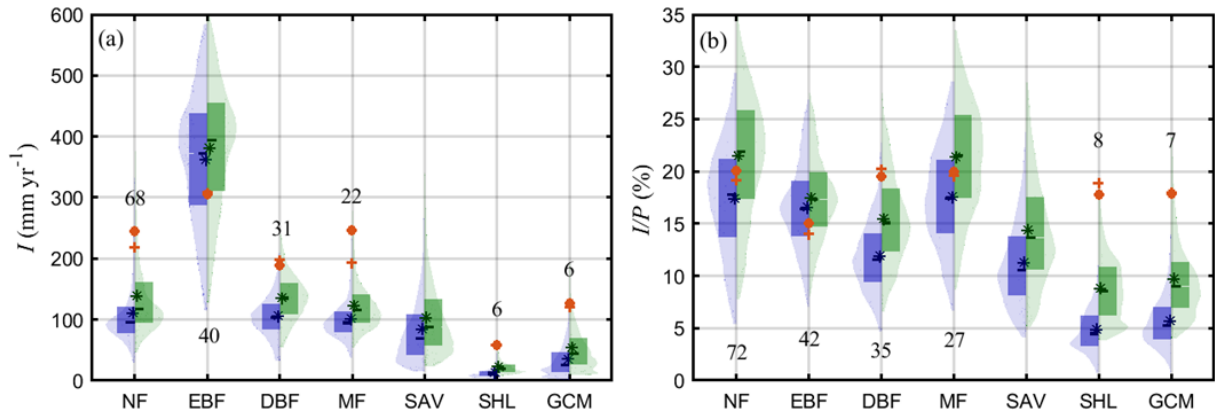


Figure 6. Global I seasonal distribution. (a, b), December–February (DJF); (c, d), March–May (MAM); (e, f), June–August (JJA) and (g, h), September–November (SON).

5.4 Interception across different vegetation types

400 To investigate differences in I for different ecosystems, Figure 7 illustrates the quantile range and kernel density for different plant functional types. Model estimates are presented both per m^2 of land surface as well as per m^2 of canopy cover, and the field data from past campaigns is shown as well. The highest I is found in evergreen broadleaf forests, with mean pixel-based estimates of $362.96 \text{ mm yr}^{-1}$ (per m^2 of land surface), at least three times larger than that for other ecosystems. This large difference relates to the high I values in tropical rainforests (Fig. 4a). Evergreen broadleaf forests is followed by needleleaf
405 forests, deciduous broadleaf forests and mixed forests, showing similar mean I values of approximately 101.74 – $111.18 \text{ mm yr}^{-1}$. Lower I values are found in sparsely vegetated land-use types, as expected: savannas, grasslands and croplands, and shrublands. When expressed in percentage of P , differences between plant functional types are lower. No large contrasts are

found between needleleaf forests, mixed forests and evergreen broadleaf forests (all around 16.58–17.56%). On the other hand, values in deciduous broadleaf forests are lower (11.91%), approaching those in savannas ecosystems (11.27%). The 410 lowest I/P is found in shrublands (4.86%), followed by grasslands and croplands (5.75%). These pixel-based I/P agree well with the estimates reported by Miralles et al. (2010) for needleleaf forests (16.1%) and deciduous broadleaf forests (12.7%), but are higher than that for evergreen broadleaf forests (10.4%). Wang-Erlandsson et al. (2014) also arrived at a comparable I/P estimate, with 18% in evergreen broadleaf forests, 17% in deciduous broadleaf forests, 18–20% in needleleaf forests, 9% in savannas, 9–13% in shrublands, grasslands and croplands, but their estimated I (in mm yr^{-1}) was generally slightly higher.



415 **Figure 7. Violin plots of I over different land-use types across the globe. (a) I in mm yr^{-1} , (b) I/P in %.** Blue violin limbs show estimates per m^2 of land surface, green per m^2 of canopy cover. The red circle and cross represent the mean and median values from field campaigns. The label in each column represents the number of field observations. Land-use types are based on the IGBP classification of MCD12C1 corresponding to 2001, including Evergreen Needleleaf Forests and Deciduous Needleleaf Forests (NF), Evergreen Broadleaf Forests (EBF), Deciduous Broadleaf Forests (DBF), Mixed Forests (MF), Woody Savannas and Savannas (SAV), Closed Shrublands and Open Shrublands (SHL), Grasslands, Croplands and Cropland/Natural Vegetation Mosaics (GCM).

Similar differences among the different land-use types are found when I is expressed per m^2 of canopy cover, but magnitudes are larger (Fig. 7). This canopy-level interception is also overall comparable to previous studies. For instance, Miralles et al. 425 (2010) found a higher canopy-level I/P in forests, however, their reported I/P per m^2 of forest of 21.8% in needleleaf forests agrees well with our study. The estimated annual I and I/P per land cover type is further compared to the reported values in field campaigns. Notice that the global estimated I is lower than the in situ measurements, except in evergreen broadleaf forests. In terms of I/P , the estimates in forests overall agree well with the field data, which indicates the average forcing precipitation might be lower than the observed precipitation from forest experiments. Both measured I and I/P over short 430 vegetated regions are much higher than the global estimates, which is consistent with the findings in field validations. In fact, the higher observed interception from short vegetation and deciduous broadleaf forests seems reasonable, as most of observations are taken in the growing season or the leafed period (Fathizadeh et al., 2018), while our estimates are the average of both the growing season and the dormant season.

5.5 Comparison to existing global datasets

435 The global multiyear (1980–2019) mean annual I estimated by the global vD–B model is 73.81 mm yr^{-1} , accounting for 10.32% of P . This value is within the range of other global estimates – e.g., the 64.06 mm yr^{-1} and 7.91% of P reported in the Community Land Model (CML) version 5 (Lawrence et al., 2019), the 115 mm yr^{-1} and 13% of P found by Wang-Erlansson et al. (2014) based on a hydrological land-surface model. Besides, this I/P is comparable to that of 10.08% reported by Zheng and Jia (2020), whereas the magnitude of I is much higher than their finding (57.06 mm yr^{-1}). This large
440 difference suggests that forcing rainfall can bring large uncertainties, which has also been found in CML5 when driven by different precipitation datasets (Lawrence et al., 2019).

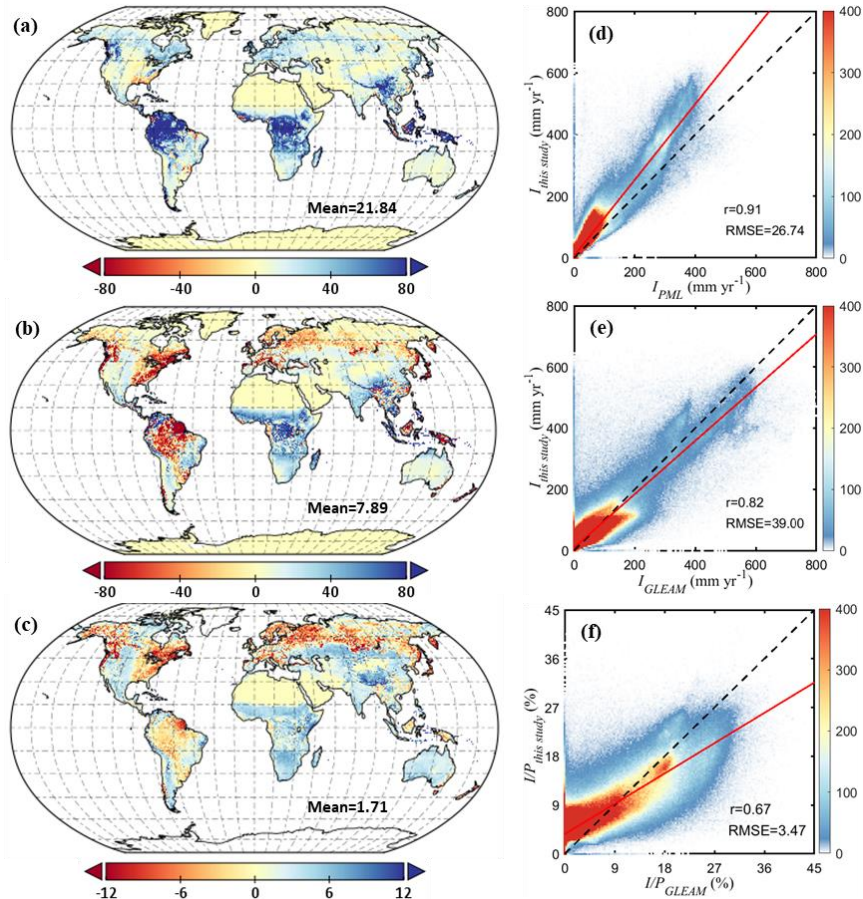
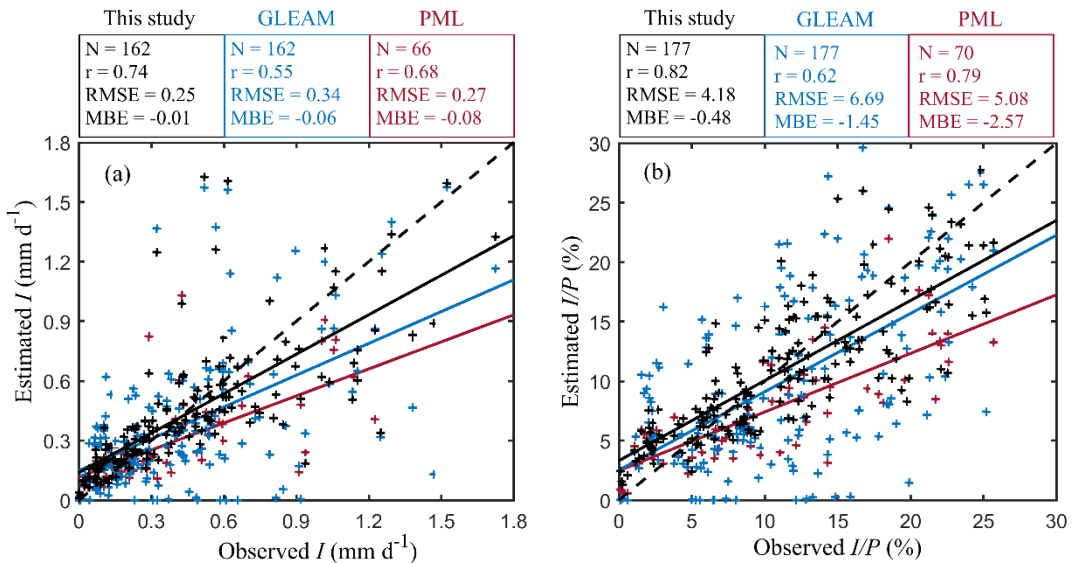


Figure 8. Comparison of rainfall interception with other global products. The left column is the spatial distribution of their differences, i.e. this study minus (a) PML I (mm yr^{-1}); (b) GLEAM I (mm yr^{-1}); (c) GLEAM I/P (%). The right column is the pixel-by-pixel scatter plot of this study versus (d) PML I (mm yr^{-1}); (e) GLEAM I (mm yr^{-1}); (f) GLEAM I/P (%), in which the red solid line represents the fitting curve, the black dashed line marks the 1-to-1 line, and colorbar represents data density.

The spatial patterns are also compared with two global interception products: PML v2 and GLEAM v3.5a (Figure 8). PML v2 is based on the same vD–B model, but with different parameterizations (Zhang et al., 2016a; 2019). Overall, annual I is in

good agreement with PML v2 estimates with a high correlation coefficient of 0.91, but higher globally with the mean difference of 21.84 mm yr⁻¹, especially in tropical regions. GLEAM v3.5a used the version of the model proposed by Valente et al. (1997), and using the same precipitation forcing as in this study, hence both I and I/P are compared here bearing in mind this dependency. In general, our interception estimates are slightly higher than GLEAM v3.5a, with the mean difference of 7.89 mm yr⁻¹ for I and 1.71% for I/P . In terms of spatial discrepancies, GLEAM v3.5a estimates are higher over Amazon forests and boreal forests, while lower in Africa, southeastern Asia and Australia. Differences in spatial patterns between both datasets ($r=0.82$ and 0.67 for I and I/P , respectively) largely come from the fact that only forest interception is estimated in GLEAM v3.5a; moreover, the phenological dynamics are not explicitly considered in GLEAM v3.5a. In addition, we validate the results of PML v2 and GLEAM v3.5a against in situ data, and compare the validation results to those of our new model formulation – see Fig. 9. Compared to PML v2 and GLEAM v3.5a, both estimated I and I/P in this study have the highest correlation coefficients and lowest mean bias errors with field observations. In evergreen broadleaf forests, similar validation results are found for estimated I , while PML v2 shows the highest correlation coefficient for I/P (Fig. S8). However, PML v2 significantly underestimates both I and I/P in evergreen broadleaf forests, especially for large events. Different from the constant of E/R in PML and the empirical relationship between R and lightning frequency in GLEAM v3.5a (Miralles et al., 2010), here use of 3-hr temporal resolution MSWEP precipitation enables a more realistic estimation of monthly averaged R (Fig. S9), which may be partly responsible for the higher model accuracy.



465

Figure 9. Field validation of rainfall interception loss from three different models. (a) I in mm d⁻¹, (b) I/P in %. Black, blue and red scatters represent the pixel-scale simulations from this study, GLEAM and PML model, respectively. Since the time series of PML v2 spans from 2003 to 2017, hence only 70 field observations can be used for validation. The solid lines in different colours are the regression lines, and the black dashed lines mark the 1-to-1 line.

In this study, we present a new global I dataset based on a revisited vD-B model (Van Dijk and Bruijnzeel, 2001b) driven by satellite-observed vegetation dynamics, potential evaporation (for short vegetation) and precipitation. In order to constrain and validate the model performance efficiently, a global synthesis of previous I field campaigns is conducted. This synthesis results in an unprecedented meta-analysis of 183 sites, and a global collection of 268 past observations. Vegetation storage 475 capacity and wet canopy evaporation rate are analysed using this synthesis dataset and used to parameterise the global model. The validation indicates the daily I estimates agree well with field observations in tall vegetation ecosystems, even compared at the precipitation event scale. The global multiyear (1980–2019) averaged annual I is 73.81 mm yr^{-1} or $10.96 \times 10^3 \text{ km}^3 \text{ yr}^{-1}$, accounting for 10.53% of continental P and representing 14.06% of continental E . Short vegetation I is also considered separately, unlike in previous global studies in which short vegetation interception was not validated (Zheng and Jia, 2020) 480 or even simulated (Miralles et al. 2010). The partitioning between tall and short vegetation benefits from the high-resolution MODIS VCF and $fPAR$ products, and the method employed here to derive cc dynamically, given the short growing season of most short vegetation ecosystems. Results indicate that short vegetation I accounts for 4.20% of continental P and contribute 485 to nearly one third of total I , a considerable amount of net water loss back to the atmosphere. However, this represents an underestimation in comparisons with field campaign results. We argue that this is likely affected by the low number of field campaigns, which are often narrowed to heavily vegetated plots within the ecosystems they sample, and the inability to validate the results over shorter vegetation types, like grasses. Meanwhile, tall vegetation accounts for 6.12% of continental P . The global I estimates in this study appear plausible according to the results of validation and spatial and seasonal analysis. 490 The global value of $10.96 \times 10^3 \text{ km}^3 \text{ yr}^{-1}$ (i.e., 10.53% of continental P) falls within the range of previous global estimates; it is higher than that from PML v2 but overall comparable to GLEAM v3.5a estimates. As expected, a strong variance is found among vegetation types and biomes, with tropical evergreen forests experiencing the largest fluxes. The seasonal variability of I is shown following the annual cycle of canopy cover, and rainfall volumes and intensity. This model will be employed as interception module in the next version (v4) of GLEAM, which is currently in development. The new global I dataset will become freely available from www.GLEAM.eu, and may serve as a benchmark for future investigations and facilitate large-scale hydrological and climate research.

Appendix A: Acronyms

Table A1. Acronyms and variable names used throughout the manuscript.

Acronym/ Symbol	Variable/Full name	Unit
<i>I</i>	Rainfall interception loss	mm
<i>P</i>	Gross rainfall	mm
<i>R</i>	Rainfall rate	mm h ⁻¹
<i>Ep</i>	potential evaporation	mm
<i>E</i>	mean evaporation rate per unit area of total land	mm h ⁻¹
<i>Ec</i>	mean evaporation rate per unit area of canopy	mm h ⁻¹
<i>S</i>	canopy storage capacity per unit area of total land	mm
<i>SV</i>	Vegetation/canopy storage capacity per unit area of canopy	mm
<i>SL</i>	leaf storage capacity	mm
<i>SS</i>	stem/trunk storage capacity	mm
<i>c</i>	canopy/vegetation cover fraction	—
<i>FF</i>	Forest Fraction	—
<i>LAI</i>	Leaf Area Index	—
<i>fPAR</i>	Fraction of absorbed Photosynthetically Active Radiation	—
<i>fPAR_{daily}</i>	daily <i>fPAR</i>	—
<i>fPAR_{mean}</i>	annual mean <i>fPAR</i>	—
<i>NDVI</i>	Normalized Difference Vegetation Index	—
<i>fIPAR</i>	Fraction of Intercepted Photosynthetically Active Radiation	—
<i>VCF</i>	Vegetation Continuous Fields	—
<i>IGBP</i>	International Geosphere–Biosphere Programme	—
<i>MSWEP</i>	Multi-Source Weighted-Ensemble Precipitation	mm
<i>SWE</i>	Snow-Water Equivalent	kg m ⁻²
<i>K(s)</i>	non-green vegetation coefficient	—
<i>P_t</i>	stemflow partitioning coefficient	—
<i>κ</i>	extinction coefficient	—
<i>C</i>	clumping index	—
<i>μ</i>	Sun zenith angle	—
<i>r</i>	correlation coefficient	—
<i>MBE</i>	mean bias error	—
<i>RMSE</i>	root-mean-square error	—

Data availability

500 The global datasets generated in this study are available upon request (Feng.Zhong@ugent.be) and will become freely available in due time via www.GLEAM.eu.

Author Contributions

F. Zhong and D. G. Miralles conceived and designed the study. F. Zhong, D. G. Miralles and A. I. J. M. van Dijk developed the model. F. Zhong did the analysis. F. Zhong and D. G. Miralles led the writing. All authors were involved in interpreting 505 the results, discussing the findings, and editing the manuscript.

Competing interests

The authors declare that they have no conflict of interest.

Acknowledgements

This work was partly funded by the European Research Council (ERC) under grant agreement no. 715254 (DRY–2–DRY).

510 This research was jointly supported by the National Natural Science Foundation of China (Grant No. U2243203), the Fundamental Research Funds for the Central Universities (Grant No. B200204029), and the China Scholarship Council (Grant No. 201906710034).

References

Acharya, S., McLaughlin, D., Kaplan, D., and Cohen, M. J.: A proposed method for estimating interception from near-surface soil moisture response, *Hydrol. Earth. Syst. Sci.*, 24, 1859–1870, <https://doi.org/10.5194/hess-24-1859-2020>, 2020.

Armstrong, R., Brodzik, M., Knowles, K., and Savoie, M.: Global monthly EASE-grid snow water equivalent climatology, version 1, National Snow and Ice Data Center Distributed Active Archive Center, Boulder, Colorado USA, doi:10.5067/KJVERY3MIBPS, 2005.

Beck, H. E., Wood, E. F., Pan, M., Fisher, C. K., Miralles, D. G., Van Dijk, A. I., McVicar, T. R., and Adler, R. F.: MSWEP 520 V2 global 3-hourly 0.1 precipitation: methodology and quantitative assessment, *Bull. Amer. Meteorol. Soc.*, 100, 473–500, <https://doi.org/10.1175/BAMS-D-17-0138.1>, 2019.

Béland, M. and Baldocchi, D. D.: Vertical structure heterogeneity in broadleaf forests: Effects on light interception and canopy photosynthesis, *Agr Forest Meteorol*, 307, <https://doi.org/10.1016/j.agrformet.2021.108525>, 2021.

Braghieri, R. K., Quaife, T., Black, E., He, L., and Chen, J.: Underestimation of global photosynthesis in Earth system 525 models due to representation of vegetation structure, *Global Biogeochem. Cycles*, 33, 1358–1369, <https://doi.org/10.1029/2018GB006135>, 2019.

Braghieri, R. K., Quaife, T., Black, E., Ryu, Y., Chen, Q., De Kauwe, M. G., and Baldocchi, D.: Influence of sun zenith angle on canopy clumping and the resulting impacts on photosynthesis, *Agr Forest Meteorol*, 291, 108065, <https://doi.org/10.1016/j.agrformet.2020.108065>, 2020.

530 Braghieri, R. K., Wang, Y., Doughty, R., Sousa, D., Magney, T., Widlowski, J.-L., Longo, M., Bloom, A. A., Worden, J., Gentine, P., and Frankenberg, C.: Accounting for canopy structure improves hyperspectral radiative transfer and sun-induced

chlorophyll fluorescence representations in a new generation Earth System model, *Remote Sens. Environ.*, 261, <https://doi.org/10.1016/j.rse.2021.112497>, 2021.

535 Calder, I., Wright, I., and Murdiyarso, D.: A study of evaporation from tropical rain forest—West Java, *J. Hydrol.*, 89, 13-31, [https://doi.org/10.1016/0022-1694\(86\)90139-3](https://doi.org/10.1016/0022-1694(86)90139-3), 1986.

Calder, I. R.: Dependence of rainfall interception on drop size: 1. Development of the two-layer stochastic model, *J. Hydrol.*, 185, 363-378, [https://doi.org/10.1016/0022-1694\(95\)02998-2](https://doi.org/10.1016/0022-1694(95)02998-2), 1996.

Carlson, T. N. and Ripley, D. A.: On the relation between NDVI, fractional vegetation cover, and leaf area index, *Remote Sens. Environ.*, 62, 241-252, [https://doi.org/10.1016/S0034-4257\(97\)00104-1](https://doi.org/10.1016/S0034-4257(97)00104-1), 1997.

540 Carlyle-Moses, D. E., Park, A. D., and Cameron, J. L.: Modelling rainfall interception loss in forest restoration trials in Panama, *Ecohydrology*, 3, 272-283, <https://doi.org/10.1002/eco.105>, 2010.

Chen, S., Chen, C., Zou, C. B., Stebler, E., Zhang, S., Hou, L., and Wang, D.: Application of Gash analytical model and parameterized Fan model to estimate canopy interception of a Chinese red pine forest, *J. For. Res.*, 18, 335-344, <https://doi.org/10.1007/s10310-012-0364-z>, 2013.

545 Chen, Y.-Y. and Li, M.-H.: Quantifying Rainfall Interception Loss of a Subtropical Broadleaved Forest in Central Taiwan, *Water*, 8, <https://doi.org/10.3390/w8010014>, 2016.

Cui, Y. and Jia, L.: A modified gash model for estimating rainfall interception loss of forest using remote sensing observations at regional scale, *Water*, 6, 993-1012, <https://doi.org/10.3390/w6040993>, 2014.

550 Cui, Y., Zhao, P., Yan, B., Xie, H., Yu, P., Wan, W., Fan, W., and Hong, Y.: Developing the Remote Sensing-Gash analytical model for estimating vegetation rainfall interception at very high resolution: A case study in the Heihe river basin, *Remote Sens.*, 9, 661, <https://doi.org/10.3390/rs9070661>, 2017.

David, J. S., Valente, F., and Gash, J. H.: Evaporation of intercepted rainfall, *Encyclopedia of hydrological sciences*, <https://doi.org/10.1002/0470848944.hsa046>, 2006.

555 de Jong, S. M. and Jetten, V.: Estimating spatial patterns of rainfall interception from remotely sensed vegetation indices and spectral mixture analysis, *Int. J. Geogr. Inf. Sci.*, 21, 529-545, <https://doi.org/10.1080/13658810601064884>, 2007.

Deguchi, A., Hattori, S., and Park, H.-T.: The influence of seasonal changes in canopy structure on interception loss: application of the revised Gash model, *J. Hydrol.*, 318, 80-102, <https://doi.org/10.1016/j.jhydrol.2005.06.005>, 2006.

560 DiMiceli, C. M., Carroll, M. L., Sohlberg, R. A., Huang, C., Hansen, M. C., and Townshend, J. R.: Annual global automated MODIS vegetation continuous fields (MOD44B) at 250 m spatial resolution for data years beginning day 65, 2000-2014, collection 5 percent tree cover, version 6, University of Maryland, College Park, MD, USA, 2017.

Dorigo, W., Dietrich, S., Aires, F., Brocca, L., Carter, S., Cretaux, J.-F., Dunkerley, D., Enomoto, H., Forsberg, R., and Güntner, A.: Closing the water cycle from observations across scales: where do we stand?, *Bull. Amer. Meteorol. Soc.*, 102, E1897-E1935, <https://doi.org/10.1175/BAMS-D-19-0316.1>, 2021.

Fan, J., Oestergaard, K. T., Guyot, A., and Lockington, D. A.: Measuring and modeling rainfall interception losses by a native Banksia woodland and an exotic pine plantation in subtropical coastal Australia, *J. Hydrol.*, 515, 156-165, <https://doi.org/10.1016/j.jhydrol.2014.04.066>, 2014.

Fathizadeh, O., Hosseini, S., Keim, R., and Boloorani, A. D.: A seasonal evaluation of the reformulated Gash interception model for semi-arid deciduous oak forest stands, *For. Ecol. Manage.*, 409, 601-613, <https://doi.org/10.1016/j.foreco.2017.11.058>, 2018.

570 Fernandes, R. P., da Costa Silva, R. W., Salemi, L. F., de Andrade, T. M. B., de Moraes, J. M., Van Dijk, A. I., and Martinelli, L. A.: The influence of sugarcane crop development on rainfall interception losses, *J. Hydrol.*, 551, 532-539, <https://doi.org/10.1016/j.jhydrol.2017.06.027>, 2017.

Finch, J. and Riche, A.: Interception losses from Miscanthus at a site in south-east England—An application of the Gash model, *Hydrol. Process.*, 24, 2594-2600, <https://doi.org/10.1002/hyp.7673>, 2010.

575 Fisher, J. B., Tu, K. P., and Baldocchi, D. D.: Global estimates of the land-atmosphere water flux based on monthly AVHRR and ISLSCP-II data, validated at 16 FLUXNET sites, *Remote Sens. Environ.*, 112, 901-919, <https://doi.org/10.1016/j.rse.2007.06.025>, 2008.

Garcia-Estringana, P., Alonso-Blázquez, N., and Alegre, J.: Water storage capacity, stemflow and water funneling in Mediterranean shrubs, *J. Hydrol.*, 389, 363-372, <https://doi.org/10.1016/j.jhydrol.2010.06.017>, 2010.

580 Gash, J.: An analytical model of rainfall interception by forests, *Q. J. R. Meteorol. Soc.*, 105, 43-55, <https://doi.org/10.1002/qj.49710544304>, 1979.

Gash, J. and Morton, A.: An application of the Rutter model to the estimation of the interception loss from Thetford forest, *J. Hydrol.*, 38, 49-58, [https://doi.org/10.1016/0022-1694\(78\)90131-2](https://doi.org/10.1016/0022-1694(78)90131-2), 1978.

585 Gash, J. and Stewart, J.: The evaporation from Thetford Forest during 1975, *J. Hydrol.*, 35, 385-396, [https://doi.org/10.1016/0022-1694\(77\)90014-2](https://doi.org/10.1016/0022-1694(77)90014-2), 1977.

Gash, J., Wright, I., and Lloyd, C. R.: Comparative estimates of interception loss from three coniferous forests in Great Britain, *J. Hydrol.*, 48, 89-105, [https://doi.org/10.1016/0022-1694\(80\)90068-2](https://doi.org/10.1016/0022-1694(80)90068-2), 1980.

Gash, J. H., Lloyd, C., and Lachaud, G.: Estimating sparse forest rainfall interception with an analytical model, *J. Hydrol.*, 170, 79-86, [https://doi.org/10.1016/0022-1694\(95\)02697-N](https://doi.org/10.1016/0022-1694(95)02697-N), 1995.

590 Ghimire, C. P., Bruijnzeel, L. A., Lubczynski, M. W., and Bonell, M.: Rainfall interception by natural and planted forests in the Middle Mountains of Central Nepal, *J. Hydrol.*, 475, 270-280, <https://doi.org/10.1016/j.jhydrol.2012.09.051>, 2012.

Ginebra-Solanellas, R. M., Holder, C. D., Lauderbaugh, L. K., and Webb, R.: The influence of changes in leaf inclination angle and leaf traits during the rainfall interception process, *Agr Forest Meteorol.*, 285, 107924, <https://doi.org/10.1016/j.agrformet.2020.107924>, 2020.

595 Hansen, M. and Song, X.: MEaSUREs Vegetation Continuous Fields (VCF) Yearly Global 0.05 Deg V001, NASA EOSDIS Land Processes 10, <https://doi.org/10.5067/MEaSUREs/VCF5KYR.001> 2017.

Hassan, S. T., Ghimire, C. P., and Lubczynski, M. W.: Remote sensing upscaling of interception loss from isolated oaks: Sardon catchment case study, Spain, *J. Hydrol.*, 555, 489-505, <https://doi.org/10.1016/j.jhydrol.2017.08.016>, 2017.

600 Herbst, M., Roberts, J. M., Rosier, P. T., and Gowing, D. J.: Measuring and modelling the rainfall interception loss by hedgerows in southern England, *Agr Forest Meteorol.*, 141, 244-256, <https://doi.org/10.1016/j.agrformet.2006.10.012>, 2006.

Holder, C. D.: Effects of leaf hydrophobicity and water droplet retention on canopy storage capacity, *Ecohydrology*, 6, 483-490, <https://doi.org/10.1002/eco.1278>, 2013.

605 Holwerda, F., Bruijnzeel, L., Scatena, F., Vugts, H., and Meesters, A.: Wet canopy evaporation from a Puerto Rican lower montane rain forest: The importance of realistically estimated aerodynamic conductance, *J. Hydrol.*, 414, 1-15, <https://doi.org/10.1016/j.jhydrol.2011.07.033>, 2012.

Hörmann, G., Branding, A., Clemen, T., Herbst, M., Hinrichs, A., and Thamm, F.: Calculation and simulation of wind controlled canopy interception of a beech forest in Northern Germany, *Agr Forest Meteorol.*, 79, 131-148, [https://doi.org/10.1016/0168-1923\(95\)02275-9](https://doi.org/10.1016/0168-1923(95)02275-9), 1996.

610 Hu, G. and Jia, L.: Monitoring of evapotranspiration in a semi-arid inland river basin by combining microwave and optical remote sensing observations, *Remote Sens.*, 7, 3056-3087, <https://doi.org/10.3390/rs70303056>, 2015.

Iida, S., Levia, D. F., Shimizu, A., Shimizu, T., Tamai, K., Nobuhiro, T., Kabeya, N., Noguchi, S., Sawano, S., and Araki, M.: Intrastorm scale rainfall interception dynamics in a mature coniferous forest stand, *J. Hydrol.*, 548, 770-783, <https://doi.org/10.1016/j.jhydrol.2017.03.009>, 2017.

Keim, R., Skaugset, A., and Weiler, M.: Storage of water on vegetation under simulated rainfall of varying intensity, *Adv. Water Resour.*, 29, 974-986, <https://doi.org/10.1016/j.advwatres.2005.07.017>, 2006.

Klaassen, W., Bosveld, F., and De Water, E.: Water storage and evaporation as constituents of rainfall interception, *J. Hydrol.*, 212, 36-50, [https://doi.org/10.1016/S0022-1694\(98\)00200-5](https://doi.org/10.1016/S0022-1694(98)00200-5), 1998.

Klaassen, W., Lankreijer, H. J. M., and Veen, A. W. L.: Rainfall interception near a forest edge, *J. Hydrol.*, 185, 349-361, [https://doi.org/10.1016/0022-1694\(95\)03011-5](https://doi.org/10.1016/0022-1694(95)03011-5), 1996.

620 Lankreijer, H., Hendriks, M., and Klaassen, W.: A comparison of models simulating rainfall interception of forests, *Agr Forest Meteorol*, 64, 187-199, [https://doi.org/10.1016/0168-1923\(93\)90028-G](https://doi.org/10.1016/0168-1923(93)90028-G), 1993.

625 Lawrence, D. M., Fisher, R. A., Koven, C. D., Oleson, K. W., Swenson, S. C., Bonan, G., Collier, N., Ghimire, B., Kampenhout, L., Kennedy, D., Kluzek, E., Lawrence, P. J., Li, F., Li, H., Lombardozzi, D., Riley, W. J., Sacks, W. J., Shi, M., Vertenstein, M., Wieder, W. R., Xu, C., Ali, A. A., Badger, A. M., Bisht, G., Broeke, M., Brunke, M. A., Burns, S. P., Buzan, J., Clark, M., Craig, A., Dahlin, K., Drewniak, B., Fisher, J. B., Flanner, M., Fox, A. M., Gentine, P., Hoffman, F., Keppel-Aleks, G., Knox, R., Kumar, S., Lenaerts, J., Leung, L. R., Lipscomb, W. H., Lu, Y., Pandey, A., Pelletier, J. D., Perket, J., Randerson, J. T., Ricciuto, D. M., Sanderson, B. M., Slater, A., Subin, Z. M., Tang, J., Thomas, R. Q., Val Martin, M., and Zeng, X.: The Community Land Model Version 5: Description of New Features, Benchmarking, and Impact of Forcing Uncertainty, *J. Adv. Model. Earth Syst.*, 11, 4245-4287, <https://doi.org/10.1029/2018MS001583>, 2019.

630 Limousin, J.-M., Rambal, S., Ourcival, J.-M., and Joffre, R.: Modelling rainfall interception in a mediterranean *Quercus ilex* ecosystem: Lesson from a throughfall exclusion experiment, *J. Hydrol.*, 357, 57-66, <https://doi.org/10.1016/j.jhydrol.2008.05.001>, 2008.

Linhoss, A. C. and Siegert, C. M.: A comparison of five forest interception models using global sensitivity and uncertainty analysis, *J. Hydrol.*, 538, 109-116, <https://doi.org/10.1016/j.jhydrol.2016.04.011>, 2016.

635 Link, T. E., Unsworth, M., and Marks, D.: The dynamics of rainfall interception by a seasonal temperate rainforest, *Agr Forest Meteorol*, 124, 171-191, <https://doi.org/10.1016/j.agrformet.2004.01.010>, 2004.

Liu, Z., Wang, Y., Tian, A., Liu, Y., Webb, A. A., Wang, Y., Zuo, H., Yu, P., Xiong, W., and Xu, L.: Characteristics of canopy interception and its simulation with a revised Gash model for a larch plantation in the Liupan Mountains, China, *J. For. Res.*, 29, 187-198, <https://doi.org/10.1007/s11676-017-0407-6>, 2018.

640 Lloyd, C. R., Gash, J. H., and Shuttleworth, W. J.: The measurement and modelling of rainfall interception by Amazonian rain forest, *Agr Forest Meteorol*, 43, 277-294, [https://doi.org/10.1016/0168-1923\(88\)90055-X](https://doi.org/10.1016/0168-1923(88)90055-X), 1988.

Lundgren, L. and Lundgren, B.: Rainfall, interception and evaporation in the Mazumbai forest reserve, West Usambara Mts., Tanzania and their importance in the assessment of land potential, *Geografiska Annaler: Series A, Physical Geography*, 61, 157-178, <https://doi.org/10.1080/04353676.1979.11879988>, 1979.

645 Luojes, K., Pulliainen, J., Takala, M., Lemmetyinen, J., Kangwa, M., Smolander, T., and Derksen, C.: Global snow monitoring for climate research: Algorithm Theoretical Basis Document (ATBD)–SWE-algorithm, Version/Revision, 1, 2013.

650 Ma, C., Li, X., Luo, Y., Shao, M., and Jia, X.: The modelling of rainfall interception in growing and dormant seasons for a pine plantation and a black locust plantation in semi-arid Northwest China, *J. Hydrol.*, 577, 123849, <https://doi.org/10.1016/j.jhydrol.2019.06.021>, 2019.

655 Majasalmi, T., Stenberg, P., and Rautiainen, M.: Comparison of ground and satellite-based methods for estimating stand-level fPAR in a boreal forest, *Agr Forest Meteorol*, 232, 422-432, <https://doi.org/10.1016/j.agrformet.2016.09.007>, 2017.

Martens, B., Miralles, D. G., Lievens, H., van der Schalie, R., de Jeu, R. A. M., Fernández-Prieto, D., Beck, H. E., Dorigo, W. A., and Verhoest, N. E. C.: GLEAM v3: satellite-based land evaporation and root-zone soil moisture, *Geosci. Model Dev.*, 10, 1903-1925, <https://doi.org/10.5194/gmd-10-1903-2017>, 2017.

Mianabadi, A., Coenders-Gerrits, M., Shirazi, P., Ghahraman, B., and Alizadeh, A.: A global Budyko model to partition evaporation into interception and transpiration, *Hydrology and Earth System Sciences* 1-32, <https://doi.org/10.5194/hess-23-4983-2019>, 2019.

Miralles, D., De Jeu, R., Gash, J., Holmes, T., and Dolman, A.: Magnitude and variability of land evaporation and its components at the global scale, *Hydrol. Earth. Syst. Sci.*, 15, 967-981, <https://doi.org/10.5194/hess-15-967-2011>, 2011a.

Miralles, D. G., Brutsaert, W., Dolman, A., and Gash, J. H.: On the use of the term “evapotranspiration”, *Water Resour. Res.*, 56, e2020WR028055, <https://doi.org/10.1029/2020WR028055>, 2020.

Miralles, D. G., Gash, J. H., Holmes, T. R., de Jeu, R. A., and Dolman, A.: Global canopy interception from satellite observations, *Journal of Geophysical Research: Atmospheres*, 115, <https://doi.org/10.1029/2009JD013530>, 2010.

660 Miralles, D. G., Holmes, T. R. H., De Jeu, R. A. M., Gash, J. H., Meesters, A. G. C. A., and Dolman, A. J.: Global land-surface evaporation estimated from satellite-based observations, *Hydrol. Earth. Syst. Sci.*, 15, 453-469, <https://doi.org/10.5194/hess-15-453-2011>, 2011b.

Molina, A. J. and del Campo, A. D.: The effects of experimental thinning on throughfall and stemflow: A contribution towards hydrology-oriented silviculture in Aleppo pine plantations, *For. Ecol. Manage.*, 269, 206-213, <https://doi.org/10.1016/j.foreco.2011.12.037>, 2012.

670 Monteith, J. L.: Evaporation and environment, *Symp. Soc. Exp. Biol.*, 205-234, 1965.

Mu, Q., Zhao, M., and Running, S. W.: Improvements to a MODIS global terrestrial evapotranspiration algorithm, *Remote Sens. Environ.*, 115, 1781-1800, <https://doi.org/10.1016/j.rse.2011.02.019>, 2011.

Mu, X., Song, W., Gao, Z., McVicar, T. R., Donohue, R. J., and Yan, G.: Fractional vegetation cover estimation by using multi-angle vegetation index, *Remote Sens. Environ.*, 216, 44-56, <https://doi.org/10.1016/j.rse.2018.06.022>, 2018.

Návar, J.: The performance of the reformulated Gash's interception loss model in Mexico's northeastern temperate forests, *Hydrol. Process.*, 27, 1626-1633, <https://doi.org/10.1002/hyp.9309>, 2013.

Návar, J.: Modeling rainfall interception components of forests: Extending drip equations, *Agr Forest Meteorol*, 279, 107704, <https://doi.org/10.1016/j.agrformet.2019.107704>, 2019.

680 Návar, J.: Modeling rainfall interception loss components of forests, *J. Hydrol.*, 584, 124449, <https://doi.org/10.1016/j.jhydrol.2019.124449>, 2020.

Návar, J. and Bryan, R. B.: Fitting the analytical model of rainfall interception of Gash to individual shrubs of semi-arid vegetation in northeastern Mexico, *Agr Forest Meteorol*, 68, 133-143, [https://doi.org/10.1016/0168-1923\(94\)90032-9](https://doi.org/10.1016/0168-1923(94)90032-9), 1994.

Návar, J., Carlyle-Moses, D. E., and Martinez, A.: Interception loss from the Tamaulipan matorral thornscrub of northeastern Mexico: an application of the Gash analytical interception loss model, *J. Arid Environ.*, 41, 1-10, <https://doi.org/10.1006/jare.1998.0460>, 1999.

Nazari, M., Sadeghi, S. M. M., Van Stan II, J. T., and Chaichi, M. R.: Rainfall interception and redistribution by maize farmland in central Iran, *J Hydrol-Reg Stud*, 27, 100656, <https://doi.org/10.1016/j.ejrh.2019.100656>, 2020.

690 Paço, T. A., David, T. S., Henriques, M. O., Pereira, J. S., Valente, F., Banza, J., Pereira, F. L., Pinto, C., and David, J. S.: Evapotranspiration from a Mediterranean evergreen oak savannah: the role of trees and pasture, *J. Hydrol.*, 369, 98-106, <https://doi.org/10.1016/j.jhydrol.2009.02.011>, 2009.

Penman, H. L.: Natural evaporation from open water, bare soil and grass, *Proceedings of the Royal Society of London. Series A. Mathematical and Physical Sciences*, 193, 120-145, <https://doi.org/10.1098/rspa.1948.0037>, 1948.

695 Pereira, F., Gash, J., David, J., and Valente, F.: Evaporation of intercepted rainfall from isolated evergreen oak trees: Do the crowns behave as wet bulbs?, *Agr Forest Meteorol*, 149, 667-679, <https://doi.org/10.1016/j.agrformet.2008.10.013>, 2009.

Pereira, F., Valente, F., David, J., Jackson, N., Minunno, F., and Gash, J.: Rainfall interception modelling: Is the wet bulb approach adequate to estimate mean evaporation rate from wet/saturated canopies in all forest types?, *J. Hydrol.*, 534, 606-615, <https://doi.org/10.1016/j.jhydrol.2016.01.035>, 2016.

700 Pérez-Suárez, M., Arredondo-Moreno, J., Huber-Sannwald, E., and Serna-Pérez, A.: Forest structure, species traits and rain characteristics influences on horizontal and vertical rainfall partitioning in a semiarid pine-oak forest from Central Mexico, *Ecohydrology*, 7, 532-543, <https://doi.org/10.1002/eco.1372>, 2014.

Reichle, R. H. and Koster, R. D.: Bias reduction in short records of satellite soil moisture, *Geophys. Res. Lett.*, 31, <https://doi.org/10.1029/2004GL020938>, 2004.

705 Reichle, R. H., Koster, R. D., De Lannoy, G. J., Forman, B. A., Liu, Q., Mahanama, S. P., and Touré, A.: Assessment and enhancement of MERRA land surface hydrology estimates, *J. Clim.*, 24, 6322-6338, <https://doi.org/10.1175/JCLI-D-10-05033.1>, 2011.

Reid, L. M. and Lewis, J.: Rates, timing, and mechanisms of rainfall interception loss in a coastal redwood forest, *J. Hydrol.*, 375, 459-470, <https://doi.org/10.1016/j.jhydrol.2009.06.048>, 2009.

710 Ringgaard, R., Herbst, M., and Friberg, T.: Partitioning forest evapotranspiration: Interception evaporation and the impact of canopy structure, local and regional advection, *J. Hydrol.*, 517, 677-690, <https://doi.org/10.1016/j.jhydrol.2014.06.007>, 2014.

Rutter, A., Morton, A., and Robins, P.: A predictive model of rainfall interception in forests. II. Generalization of the model and comparison with observations in some coniferous and hardwood stands, *J. Appl. Ecol.*, 12, 367-380, <https://www.jstor.org/stable/2401739>, 1975.

715 Rutter, A., Kershaw, K., Robins, P., and Morton, A.: A predictive model of rainfall interception in forests, 1. Derivation of the model from observations in a plantation of Corsican pine, *Agr. Meteorol.*, 9, 367-384, [https://doi.org/10.1016/0002-1571\(71\)90034-3](https://doi.org/10.1016/0002-1571(71)90034-3), 1971.

Sadeghi, S. M. M., Attarod, P., Van Stan, J. T., Pypker, T. G., and Dunkerley, D.: Efficiency of the reformulated Gash's interception model in semiarid afforestation, *Agr Forest Meteorol*, 201, 76-85, <https://doi.org/10.1016/j.agrformet.2014.10.006>, 2015.

720 Schellekens, J., Scatena, F., Bruijnzeel, L., and Wickel, A.: Modelling rainfall interception by a lowland tropical rain forest in northeastern Puerto Rico, *J. Hydrol.*, 225, 168-184, [https://doi.org/10.1016/S0022-1694\(99\)00157-2](https://doi.org/10.1016/S0022-1694(99)00157-2), 1999.

Schellekens, J., Bruijnzeel, L., Scatena, F., Bink, N., and Holwerda, F.: Evaporation from a tropical rain forest, Luquillo Experimental Forest, eastern Puerto Rico, *Water Resour. Res.*, 36, 2183-2196, <https://doi.org/10.1029/2000WR900074>, 2000.

725 Schellekens, J., Dutra, E., Martínez-de la Torre, A., Balsamo, G., van Dijk, A., Sperna Weiland, F., Minvielle, M., Calvet, J.-C., Decharme, B., Eisner, S., Fink, G., Flörke, M., Peßenteiner, S., van Beek, R., Polcher, J., Beck, H., Orth, R., Calton, B.,

Burke, S., Dorigo, W., and Weedon, G. P.: A global water resources ensemble of hydrological models: the earth2Observe Tier-1 dataset, *Earth System Science Data*, 9, 389-413, <https://doi.org/10.5194/essd-9-389-2017>, 2017.

Shi, Z., Wang, Y., Xu, L., Xiong, W., Yu, P., Gao, J., and Zhang, L.: Fraction of incident rainfall within the canopy of a pure stand of *Pinus armandii* with revised Gash model in the Liupan Mountains of China, *J. Hydrol.*, 385, 44-50, <https://doi.org/10.1016/j.jhydrol.2010.02.003>, 2010.

730 Stoy, P. C., El-Madany, T. S., Fisher, J. B., Gentine, P., Gerken, T., Good, S. P., Klosterhalfen, A., Liu, S., Miralles, D. G., Perez-Priego, O., Rigden, A. J., Skaggs, T. H., Wohlfahrt, G., Anderson, R. G., Coenders-Gerrits, A. M. J., Jung, M., Maes, W. H., Mammarella, I., Mauder, M., Migliavacca, M., Nelson, J. A., Poyatos, R., Reichstein, M., Scott, R. L., and Wolf, S.: Reviews and syntheses: Turning the challenges of partitioning ecosystem evaporation and transpiration into opportunities, *Biogeosciences*, 16, 3747-3775, <https://doi.org/10.5194/bg-16-3747-2019>, 2019.

Sulla-Menashe, D., Gray, J. M., Abercrombie, S. P., and Friedl, M. A.: Hierarchical mapping of annual global land cover 2001 to present: The MODIS Collection 6 Land Cover product, *Remote Sens. Environ.*, 222, 183-194, <https://doi.org/10.1016/j.rse.2018.12.013>, 2019.

740 Sun, X., Onda, Y., Hirata, A., Kato, H., Gomi, T., and Liu, X.: Effect of canopy openness and meteorological factors on spatial variability of throughfall isotopic composition in a Japanese cypress plantation, *Hydrol. Process.*, 32, 1038-1049, <https://doi.org/10.1002/hyp.11475>, 2018.

Tarazona, T., Santa Regina, I., and Calvo, R.: Interception, throughfall and stemflow in two forests of the " Sierra de la Demanda" in the Province of Burgos, *Pirineos*, 27-40, <http://dx.doi.org/10.3989/pirineos.1996.v147-148.135>, 1996.

745 Valente, F., David, J., and Gash, J.: Modelling interception loss for two sparse eucalypt and pine forests in central Portugal using reformulated Rutter and Gash analytical models, *J. Hydrol.*, 190, 141-162, [https://doi.org/10.1016/S0022-1694\(96\)03066-1](https://doi.org/10.1016/S0022-1694(96)03066-1), 1997.

Van Dijk, A.: The Australian Water Resources Assessment System. Technical Report 3. Landscape Model (version 0.5) Technical Description., 2010.

750 Van Dijk, A. and Bruijnzeel, L.: Modelling rainfall interception by vegetation of variable density using an adapted analytical model. Part 2. Model validation for a tropical upland mixed cropping system, *J. Hydrol.*, 247, 239-262, [https://doi.org/10.1016/S0022-1694\(01\)00393-6](https://doi.org/10.1016/S0022-1694(01)00393-6), 2001a.

Van Dijk, A. and Bruijnzeel, L.: Modelling rainfall interception by vegetation of variable density using an adapted analytical model. Part 1. Model description, *J. Hydrol.*, 247, 230-238, [https://doi.org/10.1016/S0022-1694\(01\)00392-4](https://doi.org/10.1016/S0022-1694(01)00392-4), 2001b.

755 Van Dijk, A. I., Peña-Arancibia, J. L., Wood, E. F., Sheffield, J., and Beck, H. E.: Global analysis of seasonal streamflow predictability using an ensemble prediction system and observations from 6192 small catchments worldwide, *Water Resour. Res.*, 49, 2729-2746, <https://doi.org/10.1002/wrcr.20251>, 2013.

Van Dijk, A. I., Schellekens, J., Yebra, M., Beck, H. E., Renzullo, L. J., Weerts, A., and Donchyts, G.: Global 5 km resolution estimates of secondary evaporation including irrigation through satellite data assimilation, *Hydrol. Earth. Syst. Sci.*, 22, 4959-4980, <https://doi.org/10.5194/hess-22-4959-2018>, 2018.

760 Van Dijk, A. I., Gash, J. H., Van Gorsel, E., Blanken, P. D., Cescatti, A., Emmel, C., Gielen, B., Harman, I. N., Kiely, G., and Merbold, L.: Rainfall interception and the coupled surface water and energy balance, *Agr Forest Meteorol*, 214, 402-415, <https://doi.org/10.1016/j.agrformet.2015.09.006>, 2015.

Verger, A., Baret, F., and Weiss, M.: A multisensor fusion approach to improve LAI time series, *Remote Sens. Environ.*, 115, 2460-2470, <https://doi.org/10.1016/j.rse.2011.05.006>, 2011.

765 Wallace, J. and McJannet, D.: On interception modelling of a lowland coastal rainforest in northern Queensland, Australia, *J. Hydrol.*, 329, 477-488, <https://doi.org/10.1016/j.jhydrol.2006.03.003>, 2006.

Wallace, J. and McJannet, D.: Modelling interception in coastal and montane rainforests in northern Queensland, Australia, *J. Hydrol.*, 348, 480-495, <https://doi.org/10.1016/j.jhydrol.2007.10.019>, 2008.

770 Wallace, J., Macfarlane, C., McJannet, D., Ellis, T., Grigg, A., and Van Dijk, A.: Evaluation of forest interception estimation in the continental scale Australian Water Resources Assessment–Landscape (AWRA-L) model, *J. Hydrol.*, 499, 210-223, <https://doi.org/10.1016/j.jhydrol.2013.06.036>, 2013.

Wang-Erlandsson, L., Van Der Ent, R., Gordon, L. J., and Savenije, H.: Contrasting roles of interception and transpiration in the hydrological cycle–Part 1: Temporal characteristics over land, *Earth Syst. Dynam.*, 5, 441-469, <https://doi.org/10.5194/esd-5-441-2014>, 2014.

775 Wang, D. and Wang, L.: Rainfall partitioning and its effects on regional water balances: Evidence from the conversion of traditional cropland to apple orchards in a semi-humid region, *Hydrol. Process.*, 34, 4628-4639, <https://doi.org/10.1002/hyp.13891>, 2020.

Waterloo, M., Bruijnzeel, L., Vugts, H., and Rawaqa, T.: Evaporation from *Pinus caribaea* plantations on former grassland soils under maritime tropical conditions, *Water Resour. Res.*, 35, 2133-2144, <https://doi.org/10.1029/1999WR900006>, 1999.

780 Xiao, Q. and McPherson, E. G.: Surface water storage capacity of twenty tree species in Davis, California, *J. Environ. Qual.*, 45, 188-198, <https://doi.org/10.2134/jeq2015.02.0092>, 2016.

Xiao, Q., McPherson, E. G., Ustin, S. L., and Grismer, M. E.: A new approach to modeling tree rainfall interception, *Journal of Geophysical Research: Atmospheres*, 105, 29173-29188, <https://doi.org/10.1029/2000JD900343>, 2000.

785 Yan, K., Park, T., Yan, G., Chen, C., Yang, B., Liu, Z., Nemani, R. R., Knyazikhin, Y., and Myneni, R. B.: Evaluation of MODIS LAI/FPAR product collection 6. Part 1: Consistency and improvements, *Remote Sens.*, 8, 359, <https://doi.org/10.3390/rs8050359>, 2016a.

Yan, K., Park, T., Yan, G., Liu, Z., Yang, B., Chen, C., Nemani, R. R., Knyazikhin, Y., and Myneni, R. B.: Evaluation of MODIS LAI/FPAR product collection 6. Part 2: Validation and intercomparison, *Remote Sens.*, 8, 460, <https://doi.org/10.3390/rs8060460>, 2016b.

790 Yan, T., Wang, Z., Liao, C., Xu, W., and Wan, L.: Effects of the morphological characteristics of plants on rainfall interception and kinetic energy, *J. Hydrol.*, 592, 125807, <https://doi.org/10.1016/j.jhydrol.2020.125807>, 2021.

Yang, M., Zuo, R., Li, X., and Wang, L.: Improvement Test for the Canopy Interception Parameterization Scheme in the Community Land Model, *SOLA*, 15, 166-171, <https://doi.org/10.2151/sola.2019-030>, 2019.

795 Zabret, K., Rakovec, J., and Šraj, M.: Influence of meteorological variables on rainfall partitioning for deciduous and coniferous tree species in urban area, *J. Hydrol.*, 558, 29-41, <https://doi.org/10.1016/j.jhydrol.2018.01.025>, 2018.

Zabret, K., Rakovec, J., Mikoš, M., and Šraj, M.: Influence of raindrop size distribution on throughfall dynamics under pine and birch trees at the rainfall event level, *Atmosphere*, 8, 240, <https://doi.org/10.3390/atmos8120240>, 2017.

Zeng, N., Shuttleworth, J. W., and Gash, J. H.: Influence of temporal variability of rainfall on interception loss. Part I. Point analysis, *J. Hydrol.*, 228, 228-241, [https://doi.org/10.1016/S0022-1694\(00\)00140-2](https://doi.org/10.1016/S0022-1694(00)00140-2), 2000.

800 Zhang, S.-Y., Li, X.-Y., Jiang, Z.-Y., Li, D.-Q., and Lin, H.: Modelling of rainfall partitioning by a deciduous shrub using a variable parameters Gash model, *Ecohydrology*, 11, <https://doi.org/10.1002/eco.2011>, 2018.

Zhang, Y., Kong, D., Gan, R., Chiew, F.H.S., McVicar, T.R., Zhang, Q., & Yang, Y.: Coupled estimation of 500m and 8-day resolution global evapotranspiration and gross primary production in 2002-2017. *Remote Sensing Environ.* 222, 165-182. <https://doi:10.1016/j.rse.2018.12.031>, 2019.

805 Zhang, Y., Li, X. Y., Li, W., Wu, X. C., Shi, F. Z., Fang, W. W., and Pei, T. T.: Modeling rainfall interception loss by two xerophytic shrubs in the Loess Plateau, *Hydrol. Process.*, 31, 1926-1937, <https://doi.org/10.1002/hyp.11157>, 2017.

Zhang, Y., Peña-Arancibia, J. L., McVicar, T. R., Chiew, F. H., Vaze, J., Liu, C., Lu, X., Zheng, H., Wang, Y., and Liu, Y. Y.: Multi-decadal trends in global terrestrial evapotranspiration and its components, *Sci Rep*, 6, 1-12, <https://doi.org/10.1038/srep19124>, 2016a.

810 Zhang, Z. S., Zhao, Y., Li, X. R., Huang, L., and Tan, H. J.: Gross rainfall amount and maximum rainfall intensity in 60-minute influence on interception loss of shrubs: a 10-year observation in the Tengger Desert, *Sci Rep*, 6, 1-10, <https://doi.org/10.1038/srep26030>, 2016b.

Zheng, C. and Jia, L.: Global canopy rainfall interception loss derived from satellite earth observations, *Ecohydrology*, 13, e2186, <https://doi.org/10.1002/eco.2186>, 2020.

815 Zheng, J., Fan, J., Zhang, F., Yan, S., and Xiang, Y.: Rainfall partitioning into throughfall, stemflow and interception loss by maize canopy on the semi-arid Loess Plateau of China, *Agric. Water Manage.*, 195, 25-36, <https://doi.org/10.1016/j.agwat.2017.09.013>, 2018.